Available online at www.sciencedirect.com
SCIENCE DIRECT®
Journal of volcanology and geothermal research
ELSEVIER
Journal of Volcanology and Geothermal Research 127 (2003) 219–245
www.elsevier.com/locate/jvolgeores

The mechanics of unrest at Long Valley caldera, California. 2. Constraining the nature of the source using geodetic and micro-gravity data

M. Battaglia [a,*], P. Segall [a], C. Roberts [b]

[a] *Department of Geophysics, Stanford University, Stanford, CA 94305-2215, USA*
[b] *U.S. Geological Survey, 345 Middlefield Road, MS 989, Menlo Park, CA 94025, USA*

Accepted 19 March 2003

Abstract

We model the source of inflation of Long Valley caldera by combining geodetic and micro-gravity data. Uplift from GPS and leveling, two-color EDM measurements, and residual gravity change determinations are used to estimate the intrusion geometry, assuming a vertical prolate ellipsoidal source. The U.S. Geological Survey occupied the Long Valley gravity network six times from 1980 to 1985. We reoccupied this network twice, in the summer of 1998 (33 stations), and the summer of 1999 (37 stations). Before gravity data can be used to estimate the density of the intrusion, they must be corrected for the effect of vertical deformation (the free-air effect) and changes in the water table. We use geostatistical techniques to interpolate uplift and water table changes at the gravity stations. The inflation source (a vertical prolate ellipsoid) is located 5.9 km beneath the resurgent dome with an aspect ratio equal to 0.475, a volume change from 1982 to 1999 of 0.136 km^3 and a density of around 1700 kg/m^3. A bootstrap method was employed to estimate 95% confidence bounds for the parameters of the inflation model. We obtained a range of 0.105–0.187 km^3 for the volume change, and 1180–2330 kg/m^3 for the density. Our results do not support hydrothermal fluid intrusion as the primary cause of unrest, and confirm the intrusion of silicic magma beneath Long Valley caldera. Failure to account for the ellipsoidal nature of the source biases the estimated source depth by 2.9 km (a 33% increase), the volume change by 0.019 km^3 (a 14% increase) and the density by about 1200 kg/m^3 (a 40% increase).

Keywords: Long Valley caldera; gravity; magma intrusion; ellipsoidal source; modeling

1. Introduction

Modern techniques of space geodesy, such as the Global Positioning System (GPS) and satellite radar interferometry (InSAR), now provide data of a quality, temporal and spatial density not allowed by more traditional geodetic methods. For example, it is now possible to continuously mon-

* Corresponding author. Present address: UC Berkeley Seismological Laboratory, 215 McCone Hall, Berkeley, CA 94720-4760, USA. Fax: +1-510-643-5811.
E-mail addresses: battag@seismo.berkeley.edu (M. Battaglia), segall@pangea.stanford.edu (P. Segall), croberts@usgs.gov (C. Roberts).

0377-0273/03/$ – see front matter © 2003 Elsevier B.V. All rights reserved.
doi:10.1016/S0377-0273(03)00171-9

itor volcano deformation (Dixon et al., 1997; Owen et al., 2000), or record uplift in remote volcanic areas (Amelung et al., 2000). Modeling of the pattern and rate of displacement before and during eruptions can reveal much about the physics of active volcanoes (Dvorak and Dzurisin, 1997). This is especially true when studying stratovolcanoes or basaltic shield volcanoes, since their fast, short-term deformation is well associated with magma accumulation and eruption (Tilling and Dvorak, 1993; Ewert et al., 1996; Voight et al., 1998; Nishi et al., 1999).

Interpreting geodetic measurements may be more difficult in the case of the slow, years-to-decades deformation observed at large Quaternary silicic calderas (Hill, 1998). This is well illustrated by two calderas that have a long record of measured surface displacement (Fig. 1). The caldera floor of Campi Flegrei (Fig. 1a) rose 1.7 m between 1968 and 1972, but subsided 0.22 m between 1972 and 1974. From 1982 to 1984 the caldera floor rose again (the net uplift since 1968 exceeded 3.0 m), then subsided again at a rate of 1–3 cm/yr without an eruption or clear evidence of magma intrusion (Martini et al., 1991; Barberi et al., 1996). Yellowstone caldera (Fig. 1b) has shown a similar behavior. Uplift of resurgent domes within the Yellowstone caldera started sometime after 1923, reaching a total uplift of 90 cm; in 1984 the uplift reversed to subsidence at a rate of 1–2 cm/yr (Dzurisin et al., 1994). Wicks et al. (1998) showed that between 1992 and 1996 deformation in Yellowstone changed again from subsidence to uplift, with deformation migrating from one resurgent dome to the other.

Several authors have proposed that caldera unrest may be caused by aqueous fluid intrusions, or interaction between the hydrothermal system and magma intrusions (Dzurisin et al., 1990, 1994; Bonafede, 1991; De Natale et al., 1991; Wicks et al., 1998; Orsi et al., 1999). Geodesy alone cannot discriminate between magma and aqueous fluid intrusion. Gravity measurements, however, can constrain the mass of the intrusion. Combined geodesy and gravity measurements can be used to infer the density of the intrusive fluids, and can better constrain the deformation source (Berrino et al., 1992; Rymer, 1994). Given the significant density difference between silicate melts (-2500 kg/m^3) and hydrothermal fluids (-1000 kg/m^3), it is reasonable to use density estimates from gravity to distinguish between these two possible sources of caldera unrest.

When trying to combine geodesy and microgravity to study the physics of active volcanoes there are several challenges that need to be addressed. The gravity change Δg we measure in the field is the superposition of several effects (Fig. 2):

$$\Delta g = \left(\frac{\partial g}{\partial z}\right)_0 h + 4\pi\rho_w \phi \delta z + \Delta g_D + \Delta g_R \qquad (1)$$

i.e. the free-air effect proportional to the uplift h ($(\partial g/\partial z)_0 = 308.6$ μGal/m is the average free-air gradient); the water table correction ($4\pi\rho_w\phi\delta z =$ 42 μGal/m) proportional to the porosity ϕ and water table change δz of an unconfined aquifer

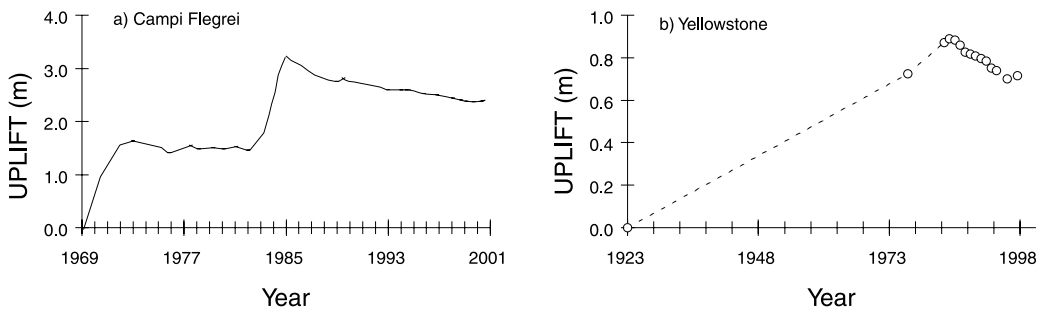

Fig. 1. (a) Campi Flegrei (Italy): elevation changes near Pozzuoli, central caldera floor, benchmark 25 (Barberi et al., 1996; Del Gaudio et al., 2001). (b) Yellowstone caldera (WY): elevation changes at Sour Creek dome, benchmark B11_1923 (Dzurisin et al., 1994; Wicks et al., 1998).

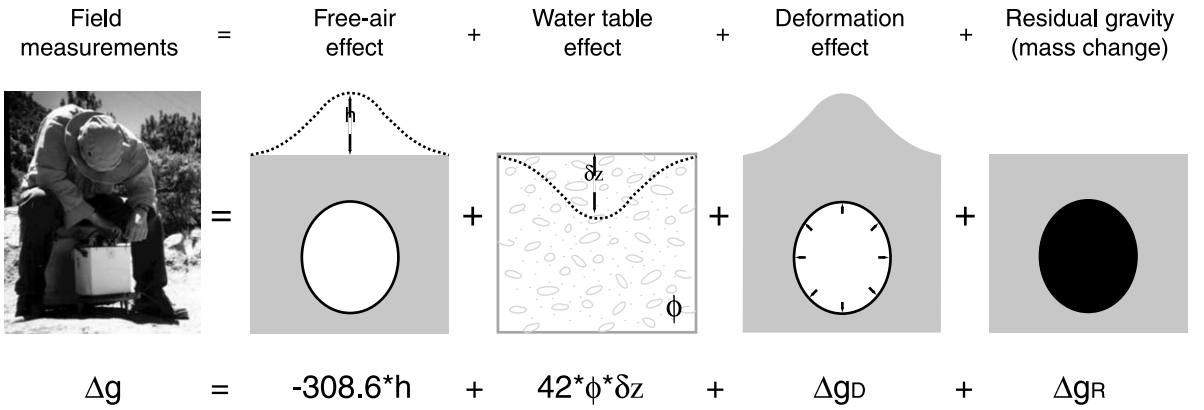

Fig. 2. The different effects that compose the gravity signal measured in the field. All constants are in μGal/m, h is the vertical displacement, ϕ the porosity and δz the water table change. The deformation effect Δg_D is zero for changes in gravity resulting from expansion of a isotropic source in a homogeneous elastic half-space (Walsh and Rice, 1979).

(see Appendix 1); Δg_D takes into account coupling effects between gravity and elastic deformation (e.g. Bonafede and Mazzanti, 1998). The residual gravity Δg_R is then dependent on the mass change accompanying the deformation (Jachens and Roberts, 1985; Eggers, 1987). Here we use the theoretical value of the free-air gradient rather than the local observed value (e.g. Berrino et al., 1992) to compute the free-air gravity correction. Variations in the free-air gradient are mainly due to local topography and density anomalies (e.g. Kuo et al., 1969). These local sources of perturbation will displace with the long-wavelength caldera uplift. Thus, the theoretical free-air gradient more accurately represents the change in gravity due to uplift (Jachens, personal communication). In addition, the vertical gradient of gravity at a point is difficult to measure and errors can be easily introduced. The deformation effect Δg_D is zero for changes in gravity resulting from an isotropic source in a homogeneous elastic half-space (Walsh and Rice, 1979). We neglect second-order effects associated with coupling between gravity and elastic deformation (e.g. Walsh and Rice, 1979; Wang, 1997). To estimate the residual gravity, and from this the mass of the intrusion, we must know the uplift h, porosity ϕ and water table change δz at every gravity station. This is often not an easy task because gravity and geodetic benchmarks rarely coincide. Porosity and water level data may be sparse or non-existent at gravity stations. The standard approach is to develop survey strategies to minimize the water table correction rather than trying to estimate it (Rundle and Whitcomb, 1986; McKee et al., 1989; Arnet et al., 1997).

Another critical choice in constraining the deformation source is the model used to invert the geodetic and gravity data. The most common approach is to invert gravity and uplift data using the well-known isotropic point source in a homogeneous elastic half-space (McKee et al., 1989; Berrino, 1994; Battaglia et al., 1999; Rymer and Williams-Jones, 2000). A variety of different geometries, including point sources, finite spheres and sills, have very similar vertical deformation patterns (e.g. Dieterich and Decker, 1975). We show here that uncertainty in source shape can lead to an inaccurate estimate of the depth and thus density of the intrusion.

This paper has two goals. The first is to provide an answer to the numerous challenges faced when applying geodetic and gravity data to the study of the physics of volcanoes. We use geostatistics (e.g. Journel, 1989) to interpolate water table changes and uplift (and estimate the corresponding interpolation uncertainties) at gravity stations where these measurements are lacking (see Appendix 2 for more details). Geographical Information System software allows us to associate each gravity benchmark with a lithology, and thus estimate the porosity of the site. The second goal is to use

geodetic and gravity data to better constrain the source of deformation at Long Valley caldera. Although magma intrusion has been suggested by several authors to explain caldera deformation, seismicity and gas emissions (Savage and Cockerham, 1984; Savage et al., 1987; Hill et al., 1990; Sorey et al., 1993; Langbein et al., 1995), direct estimates of the mass and density of the intrusion have only become available recently (Battaglia et al., 1999). We show that a simple isotropic point source model yields misleading estimates of the depth and density of the intrusion if the source geometry departs from a spherical shape. Compared to our previous work (Battaglia et al., 1999) we: (1) present twice as much gravity data, adding new data from the July 1999 survey, with a consequent reduction of the errors in the Δg measurements; (2) increase the number of gravity sites with a direct measurement of uplift from a GPS survey in July 1999 (see Battaglia et al., 2003 – this issue); (3) improve the inflation source model by including two-color EDM data to better constrain the source shape (see Battaglia et al., 2003 – this issue); (4) invert geodetic and gravity data using ellipsoidal source models developed by Clark et al. (1986) and Yang et al. (1988).

2. Long Valley caldera geodetic and gravity surveys

The results of leveling and trilateration surveys suggest that little if any deformation occurred in Long Valley caldera before 1980, when intense seismic activity marked the beginning of unrest (Bailey and Hill, 1990). Results of frequent leveling and two-color EDM surveys in the following years indicated the continuous rise of the caldera center at variable rates. Deformation rates peaked during the second half of 1997 (Fig. 3). The last complete leveling of the caldera was conducted in 1992. We surveyed 44 of the existing leveling monuments in Long Valley in July 1999, using dual-frequency GPS receivers, to bring up to date the measurement of the vertical deformation field within the caldera. According to this survey, the resurgent dome stands 0.74 ± 0.07 m higher than in 1980 (Battaglia et al., 2003 – this issue),

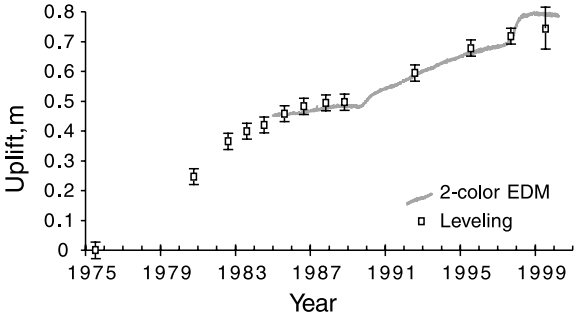

Fig. 3. Rise of caldera center from 1975 to present. The horizontal deformation along the CASA-KRAK baseline provides a proxy for the vertical deformation at the resurgent dome (benchmark W911). The July 1999 uplift is based on GPS measurements. Modified from Battaglia et al. (2003 – this issue).

although according to the two-color EDM data there has been a slight contraction, and thus inferred subsidence since mid-1998 (Fig. 3). Several sources of deformation have been identified in Long Valley caldera. The principal ones are the intrusion of a magma body beneath the resurgent dome, and right-lateral strike-slip in the south moat of the caldera (Savage et al., 1987; Langbein et al., 1995). In addition, there is evidence of dike intrusion beneath the south moat (Savage and Cockerham, 1984; Langbein, 1995) and Mammoth Mountain (Hill et al., 1990; Langbein et al., 1995).

The Long Valley caldera gravity monitoring network is centered near Tom's Place (the primary reference station) and extends from the Sierra Nevada west of Lee Vining, CA, southeastward to a station in the White Mountains east of Bishop, CA. Most of the stations outside of Long Valley caldera are on crystalline bedrock outcrops, while volcanic flows or sediments underlie the stations within the caldera. The U.S. Geological Survey (USGS) occupied the network every summer from 1980 to 1985 (Jachens and Roberts, 1985; Roberts et al., 1988).

Earlier efforts at detecting and interpreting gravity changes in the Long Valley area were limited by the small amplitude of the accumulated signal, and the difficulty in correcting for the water table effect (Jachens and Roberts, 1985). Results from the 1998 gravity survey demonstrate

Table 1
Data from the June 1982 (Roberts et al., 1988), July 1998 and July 1999 gravity surveys in Long Valley caldera; gravity changes from 1982 to 1998 (1998–82), and from 1982 to 1999 (1999–82)

Station	*X* (UTM)	*Y* (UTM)	June 1982	July 1998	July 1999	1998–82	1999–82
HW 395							
X123	326 136.14	4 178 629.24	275 298 ± 4	275 246 ± 3	275 256 ± 15	−52 ± 5	−42 ± 16
MLEQ03A	328 462.44	4 177 303.91	192 608 ± 8	192 529 ± 19	192 512 ± 10	−79 ± 20	−96 ± 13
D916	328 094.57	4 174 458.65	242 451 ± 5		242 408 ± 9		−43 ± 11
Y123	328 785.78	4 172 912.38	240 707 ± 8	240 641 ± 3	240 655 ± 8	−66 ± 8	−52 ± 11
12DOR75	329 558.81	4 171 897.32	242 333 ± 5		242 215 ± 12		−118 ± 13
MLEQ02	330 200.44	4 169 630.69	258 850 ± 3	258 745 ± 8	258 728 ± 5	−106 ± 9	−123 ± 6
FLOW	332 710.85	4 166 338.21	264 465 ± 3	264 387 ± 10	264 386 ± 6	−78 ± 10	−79 ± 7
A124RST	335 575.89	4 166 125.40	268 816 ± 7		268 771 ± 10		−45 ± 12
CONVICT	340 248.21	4 164 402.24	284 162 ± 4	284 116 ± 10	284 069 ± 4	−46 ± 10	−93 ± 5
6DOR75	342 544.68	4 161 183.78	299 354 ± 6	299 336 ± 6	299 308 ± 3	−18 ± 9	−46 ± 7
D124	344 672.23	4 159 700.73	301 911 ± 4	301 852 ± 6	301 880 ± 9	−59 ± 7	−31 ± 10
E124	347 595.03	4 158 658.68	283 020 ± 5	283 001 ± 2	282 997 ± 5	−19 ± 5	−23 ± 7
MLEQB1	350 322.53	4 158 509.15	311 968 ± 3	311 958 ± 5	311 964 ± 5	−10 ± 6	−4 ± 6
Big loop							
E916	329 965.18	4 179 626.16	290 229 ± 4		290 166 ± 6		−63 ± 7
24DOR75	336 407.05	4 178 663.26	286 631 ± 5	286 564 ± 9	286 548 ± 12	−67 ± 10	−83 ± 13
39DOR75	340 137.81	4 176 492.17	276 264 ± 5	276 218 ± 23	276 204 ± 6	−46 ± 24	−60 ± 8
2JD1952	340 271.97	4 170 662.09	277 161 ± 4	277 119 ± 10	277 137 ± 6	−42 ± 11	−24 ± 7
MLEQ01	340 381.90	4 168 129.20	275 966 ± 4	275 927 ± 11	275 930 ± 3	−39 ± 12	−36 ± 5
1JD1952	340 232.08	4 166 311.72	279 875 ± 4	279 815 ± 9	279 815 ± 1	−60 ± 9	−60 ± 4
Small loop							
12JCM82	330 078.01	4 175 261.24	250 950 ± 6	250 874 ± 4	250 854 ± 8	−76 ± 7	−96 ± 10
15JCM82	332 778.60	4 174 484.55	234 052 ± 6	233 979 ± 6	233 963 ± 4	−73 ± 8	−89 ± 7
16JCM82	333 520.47	4 173 659.22	253 378 ± 3	253 316 ± 7	253 265 ± 5	−62 ± 8	−113 ± 6
17JCM82	333 626.24	4 171 903.23	257 768 ± 6	257 680 ± 5	257 712 ± 5	−88 ± 8	−56 ± 8
22JCM82	332 215.26	4 171 065.92	236 305 ± 6	236 217 ± 4	236 233 ± 7	−88 ± 7	−72 ± 9
23JCM82	331 824.28	4 170 063.72	237 917 ± 5	237 810 ± 3	237 834 ± 5	−107 ± 6	−83 ± 7
Antelope Valley Rd							
25JCM82	336 091.36	4 172 531.07	266 463 ± 7	266 366 ± 4	266 348 ± 9	−97 ± 8	−115 ± 11
Benton Crossing							
3JD1952	342 363.47	4 172 531.10	276 013 ± 6	275 983 ± 13	275 968 ± 4	−30 ± 14	−45 ± 7
4JD1952	344 644.06	4 173 719.96	285 712 ± 4	285 708 ± 6	285 682 ± 4	−4 ± 7	−30 ± 6
HW 203							
5JCM82	324 333.68	4 169 320.30	206 986 ± 7		206 927 ± 13		−59 ± 15
3JCM82	327 207.40	4 168 305.09	232 661 ± 4	232 605 ± 7	232 581 ± 9	−56 ± 8	−80 ± 10
2JCM82	328 808.72	4 167 627.96	242 013 ± 6	241 936 ± 12	241 914 ± 8	−77 ± 14	−99 ± 10
Control stations							
MLEQ06	337 854.09	4 168 400.36	311 297 ± 4	311 294 ± 10	311 292 ± 4	−3 ± 11	−5 ± 6
MLEQ11	328 744.70	4 181 127.85	128 305 ± 6	128 300 ± 7	128 294 ± 4	−5 ± 9	−11 ± 7
MLEQ13	329 228.97	4 166 176.19	324 252 ± 4	324 249 ± 6	324 254 ± 5	−3 ± 7	2 ± 6
More stations with alternate							
HOT	309 973.59	4 200 269.54	272 917 ± 4	272 854 ± 11	272 841 ± 4	−63 ± 12	−76 ± 6
MLEQ05	346 515.77	4 146 613.81	287 340 ± 4	287 301 ± 8	287 329 ± 6	−39 ± 9	−11 ± 7
MLEQ14	358 851.07	4 167 982.14	244 579 ± 4	244 493 ± 10	244 460 ± 12	−86 ± 10	−119 ± 12

All values are given in μGal and errors are 1 S.D. Benchmark coordinates in UTM (NAD27). See Fig. 4 for benchmark location.

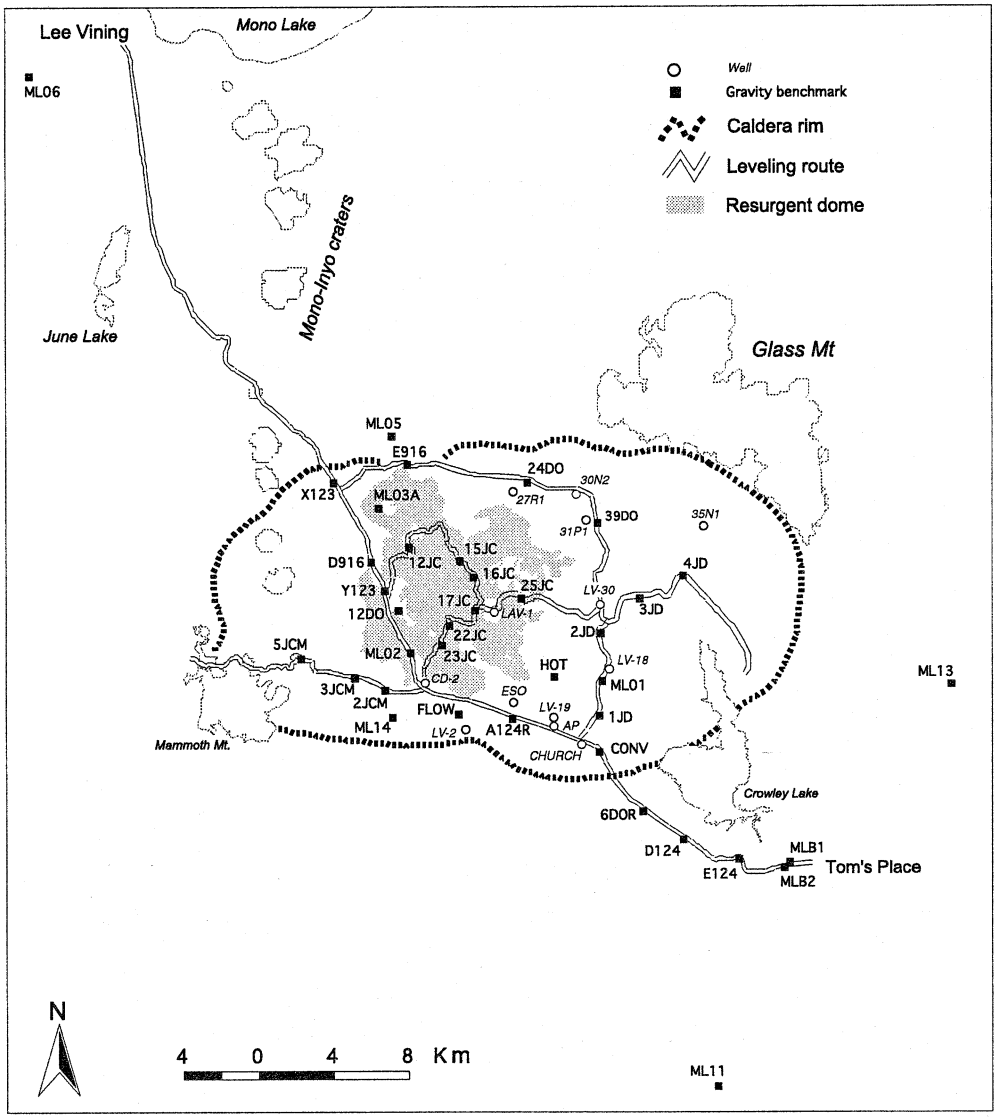

Fig. 4. Gravity stations occupied in Long Valley caldera in July 1998 and July 1999 (see Table 1). The network base station is MLEQB2 (Tom's Place). MLE06 (Lee Vining), MLEQ11 (Rock Creek) and MLEQ13 (Benton Crossing) are the network control stations. Only 13 shallow wells of the hydrologic monitoring network have been surveyed both in 1982, 1998 and 1999.

the intrusion of magma beneath the resurgent dome and do not support perturbation in the hydrothermal system as the primary cause of uplift (Battaglia et al., 1999).

We occupied 32 gravity stations in 1998 and 37 stations in 1999 (Fig. 4 and Table 1). Gravity measurements were carried out using two LaCoste and Romberg gravimeters, models D26 and G8, simultaneously. These two gravity meters are the original meters used previously by the USGS in Long Valley. They were refurbished and calibrated by LaCoste and Romberg in the spring of 1998. We measured the relative gravity at selected stations along closed loops starting from Tom's Place (benchmark MLEQB2), the primary reference station. Every station was occupied

Table 2
Water table correction for the 1998 and 1999 surveys

	Outcrop	ϕ	1998 change (m)	1998 correction (μGal)	1999 change (m)	1999 correction (μGal)
HW 395						
X123	Flow	0.10	−0.60 ± 1.56	−3 ± 7	0.07 ± 0.79	0 ± 3
MLEQ03A	Flow	0.10	−0.60 ± 1.63	−3 ± 7	0.07 ± 0.73	0 ± 3
D916	Sediments	0.45			0.07 ± 0.84	1 ± 16
Y123	Sediments	0.45	−0.36 ± 1.34	−7 ± 25	0.07 ± 0.93	1 ± 18
12DOR75	Sediments	0.45			0.07 ± 0.90	1 ± 17
MLEQ02	Flow	0.10	−0.37 ± 3.25	−2 ± 14	−1.34 ± 1.00	−6 ± 7
FLOW	Flow	0.10	−0.21 ± 0.16	−1 ± 1	−2.62 ± 0.86	−11 ± 12
A124RST	Sediments	0.45			−1.57 ± 0.76	−30 ± 16
CONVICT	Sediments	0.45	−0.05 ± 0.17	−1 ± 3	−0.44 ± 0.13	−8 ± 3
6DOR75	Sediments	0.45	−0.01 ± 1.21	0 ± 23	−0.49 ± 0.48	−9 ± 9
D124	Sediments	0.45	0.01 ± 0.80	0 ± 15	0.12 ± 0.77	2 ± 15
E124	Flow	0.10	0.38 ± 1.37	2 ± 6	−0.32 ± 0.67	−1 ± 3
MLEQB1	Granite	0.05	0.16 ± 0.94	0 ± 2	−0.61 ± 0.68	−1 ± 3
Big loop						
X123	Flow	0.10	−0.60 ± 1.56	−3 ± 7	0.07 ± 0.79	0 ± 3
E916	Flow	0.10			−0.25 ± 0.77	−1 ± 3
24DOR75	Sediments	0.45	0.11 ± 0.19	2 ± 4	−0.62 ± 0.85	−12 ± 16
39DOR75	Sediments	0.45	−0.15 ± 0.13	−3 ± 3	−0.62 ± 0.77	−12 ± 15
2JD1952	Sediments	0.45	−0.32 ± 0.22	−6 ± 4	−0.61 ± 0.84	−12 ± 16
MLEQ01	Flow	0.10	0.16 ± 0.22	1 ± 1	−0.61 ± 0.37	−3 ± 3
1JD1952	Sediments	0.45	−0.09 ± 0.95	−2 ± 18	−0.69 ± 0.55	−13 ± 11
Small loop						
12JCM82	Flow	0.10	−0.35 ± 0.72	−1 ± 3	0.07 ± 0.76	0 ± 3
15JCM82	Flow	0.10	−0.32 ± 0.67	−1 ± 3	0.07 ± 0.64	0 ± 3
16JCM82	Flow	0.10	−0.36 ± 0.44	−1 ± 2	0.07 ± 0.43	0 ± 2
17JCM82	Flow	0.10	−0.36 ± 0.29	−1 ± 2	0.07 ± 0.64	0 ± 3
22JCM82	Flow	0.10	−0.36 ± 1.68	−1 ± 7	0.07 ± 0.86	0 ± 4
23JCM82	Flow	0.10	−0.48 ± 2.76	−2 ± 12	−1.09 ± 0.95	−5 ± 6
Antelope Valley Rd						
25JCM82	Flow	0.10	−0.19 ± 0.42	−1 ± 2	0.07 ± 0.57	0 ± 2
Benton Crossing						
3JD1952	Sediments	0.45	0.17 ± 0.53	3 ± 10	−0.61 ± 0.83	−12 ± 16
4JD1952	Sediments	0.45	0.01 ± 0.65	0 ± 12	−0.58 ± 0.92	−11 ± 17
HW 203						
5JCM82	Sediments	0.45			−2.62 ± 0.75	−50 ± 18
3JCM82	Sediments	0.45	−0.21 ± 1.83	−4 ± 35	−2.62 ± 1.05	−50 ± 23
2JCM82	Sediments	0.45	−0.21 ± 3.00	−4 ± 57	−2.62 ± 0.95	−50 ± 21
More stations with alternate						
HOT	Flow	0.10	−0.10 ± 0.29	0 ± 1	−0.69 ± 0.83	−3 ± 5
MLEQ05	Granite	0.05	−0.60 ± 0.86	−1 ± 3	−0.25 ± 0.91	−1 ± 2
MLEQ14	Flow	0.10	−0.21 ± 2.49	−1 ± 10	−2.62 ± 1.06	−11 ± 12

Porosity ϕ is assigned to each site based on the local rock type (e.g. Sorey et al., 1978). Labels for water table changes δz are *1998 change* and *1999 change*. Water table correction labels are *1998 correction* and *1999 correction*. Errors are 1 S.D.

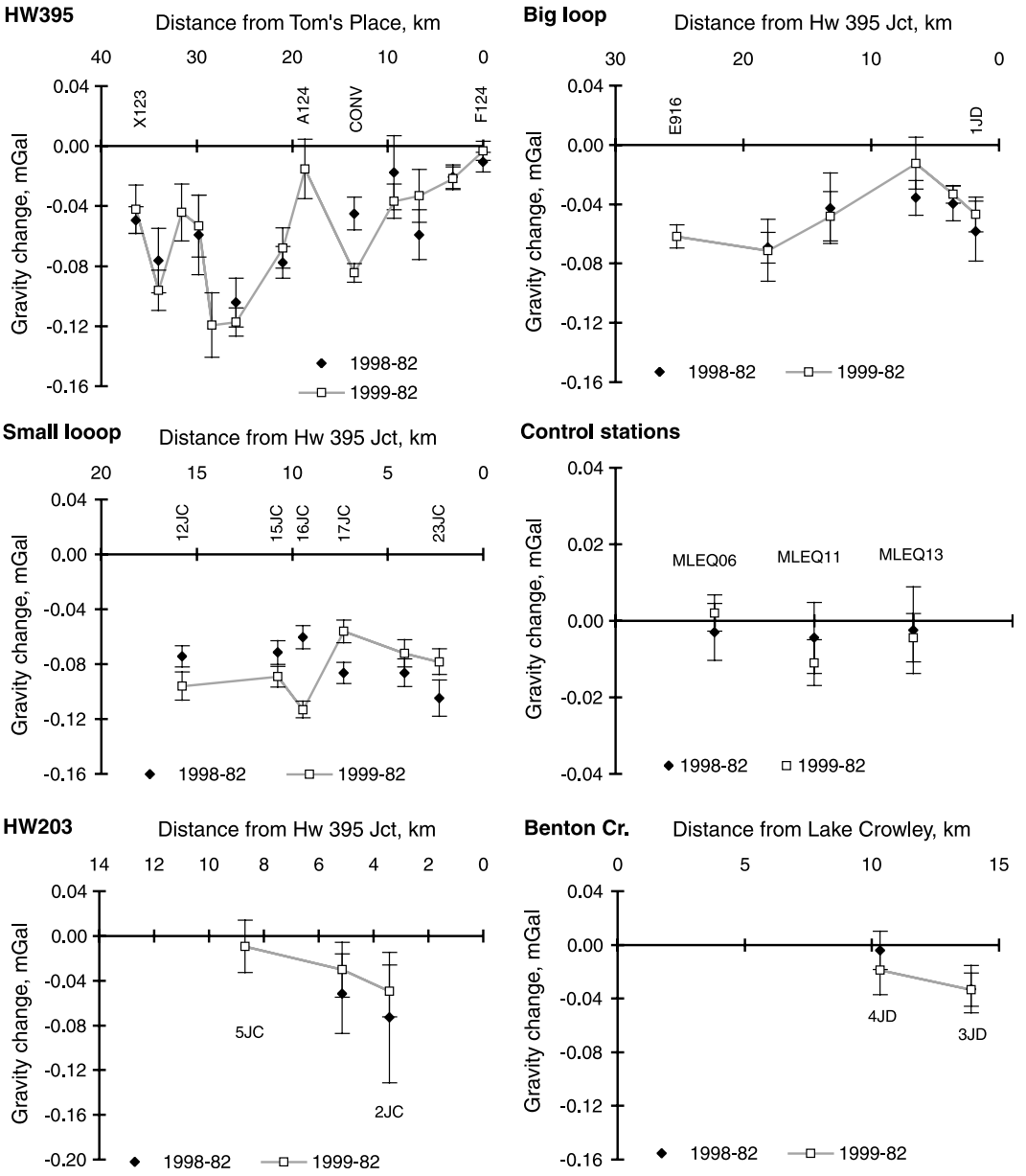

Fig. 5. Gravity changes from 1982 to 1998 (1998–82) and from 1982 to 1999 (1999–82) corrected for the water table fluctuations (see Table 2). Error bars correspond to 1 S.D.

twice. Several stations of the gravity network had an alternate benchmark; so many points of the gravity network were measured four times a day using two different gravimeters. Data reduction included the removal of solid Earth-tides and daily gravimeter drift following the methods described in Jachens et al. (1982). The data were then examined for evidence of sudden changes of reading (or 'tares') and corrections were applied when necessary. Finally, the measured relative gravity values were averaged using a least-squares method to obtain one gravity determina-

tion at each station, using software developed at the USGS, Menlo Park, CA. The average error (1 standard deviation) for the gravity surveys was ±8 μGal in 1998 and ±7 μGal in 1999. These estimates include contributions from errors in the tide correction and drift removal, as well as uncertainties in gravimeter readings caused by fluctuations in ambient temperature, vibrations experienced by the instruments, and errors in adjusting the meter bubble level (Jachens, 1979).

3. Water table correction and gravity changes

Before we can interpret the measured temporal gravity changes (Table 1), it is necessary to correct them for the variation in the level of the water table. This means that we must know the value of porosity ϕ and water table change δz at every gravity station occupied during the 1998 and 1999 survey. Porosity is assigned to each site based on the local rock type (see Table 2). The water table level is measured in shallow wells (Fig. 4) three times a year (usually in May, July and November), and the first complete survey of the hydrologic monitoring network of Long Valley caldera dates back to 1982 (Howle and Farrar, 1996). Hydrologic data are sparse or non-existent at several monitoring wells before 1982 (Howle and Farrar, 1996), making it practically impossible to compute the water table correction for gravity data recorded in 1980 and 1981.

To estimate the water table correction for the 1982–1998 and 1982–1999 intervals, we must address two problems. First, water wells and gravity stations are not generally close to one another (Fig. 4). We can solve this problem by interpolating water table changes at gravity stations where these measurements are lacking. Second, even if there is a large hydrologic data set collected in the past 20 years, the number of shallow wells surveyed both in 1982 and 1998, or 1982 and 1999 is small (Fig. 4), and it is not possible to use standard geostatistical spatial models to interpolate. The solution is to develop an interpolation scheme using a geostatistical space–time model (Rouhani and Myers, 1990; Kyriakidis and Journel, 1999) that includes information from all the available hydrological data (see Appendix 2 for more details on the geostatistical model). The model was implemented using the ordinary kriging algorithm provided by the GSLIB computer code (Deutsch and Journel, 1998). The interpolation error is estimated through sequential Gaussian simulation. Gaussian simulation is the process of drawing alternative, equally probable, joint realizations of a random variable (in this case the change in water table depth at a given location) assuming that the variable follows a multivariate Gaussian distribution. All the realizations fit the existing data exactly, and the variance of a set of simulated values at a given site provides a measure of the interpolation error (Goovaerts, 1997).

The calculated water table corrections are given in Table 2. The net effect on the gravity measurements is small for the 1982–1998 interval, typically 1–4 μGal, the largest correction being −7 μGal at a site on caldera fill sediments. The correction is more significant for the 1982–1999 period, typically 1– 12 μGal, the largest correction being −50 μGal for two sites on glacial moraine sediments and one site on loose volcanics. The uncertainties in the water table correction depend on how close the site is to a monitoring well, the quality of the data from that well, and the porosity. Estimated errors, based on simulation of the water table level histories and assuming a 10% uncertainty in the porosity, range from a low of 3 μGal on granite and rhyolite outcrops to a maximum of 57 μGal for one site on glacial moraine sediments in the 1982–1998 interval.

The internal consistency of the gravity measurements before and after the water table correction provides a measure of the efficacy of the interpolated corrections. The two-color EDM data indicate little or no deformation between the summer of 1998 and 1999. Thus we expect the 1982–1998 and 1982–1999 gravity changes to agree. We find the water table correction significantly improves the agreement between the 1998 and 1999 surveys. Whereas $\chi^2 = 128$ before the water table correction, it decreases to $\chi^2 = 68$ after the water table correction (here χ^2 is defined as the weighted sum of the squares of the difference between the 1999 and 1998 gravity determinations). Gravity

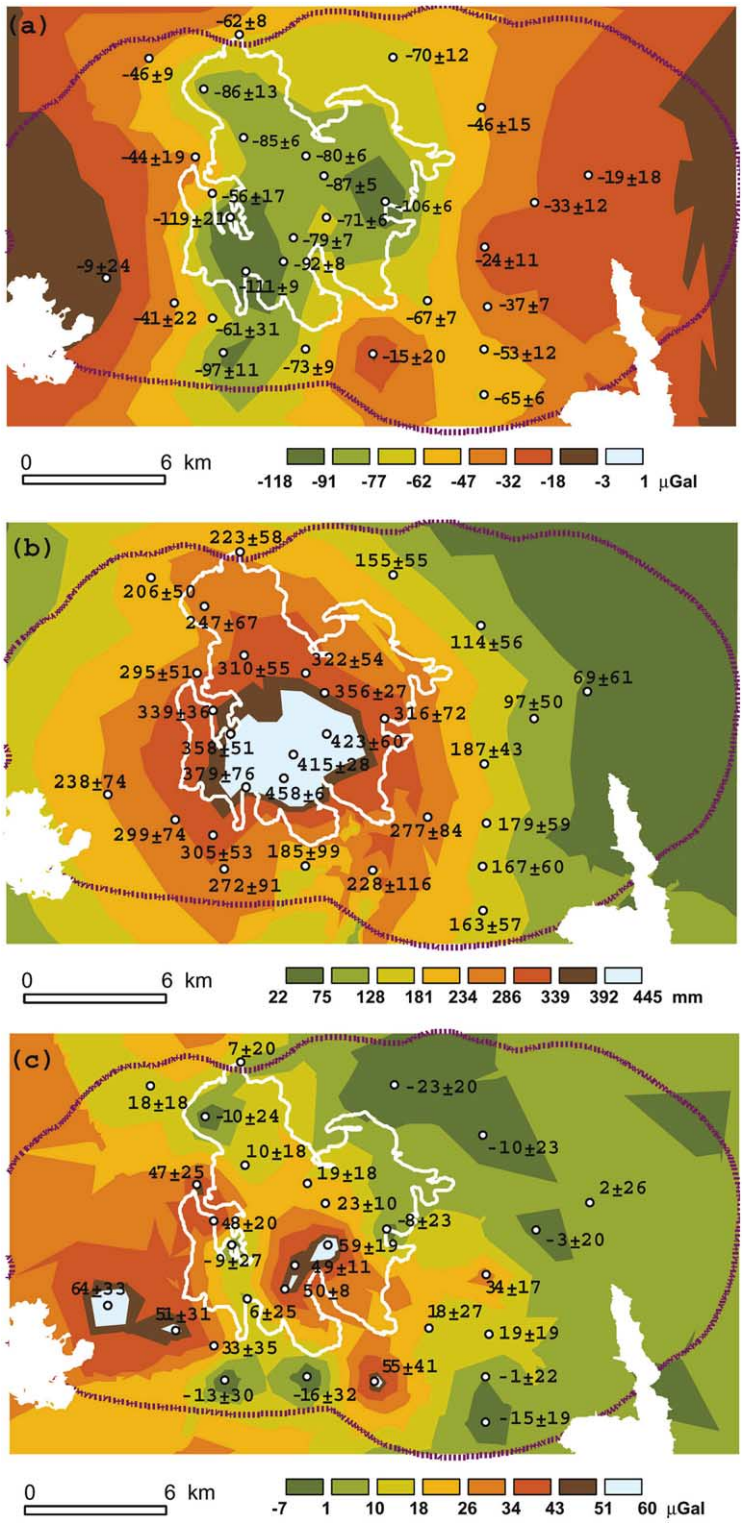
(a)
-62±8
-46±9
-70±12
-86±13
-46±15
-85±6
-44±19
-80±6
-87±5
-19±18
-56±17
-106±6
-33±12
-119±21
-71±6
-79±7
-9±24
-92±8
-24±11
-111±9
-37±7
-41±22
-61±31
-67±7
-15±20
-53±12
-97±11
-73±9
-65±6
0
6 km
-118 -91 -77 -62 -47 -32 -18 -3 1 μGal
(b)
223±58
155±55
206±50
247±67
114±56
295±51
310±55
322±54
69±61
356±27
339±36
316±72
97±50
423±60
358±51
187±43
415±28
379±76
238±74
458±6
277±84
179±59
299±74
305±53
185±99
167±60
272±91
228±116
163±57
0
6 km
22 75 128 181 234 286 339 392 445 mm
(c)
7±20
-23±20
18±18
-10±24
-10±23
10±18
47±25
19±18
2±26
23±10
-8±23
48±20
-3±20
59±19
-9±27
49±11
64±33
34±17
50±8
51±31
6±25
18±27
19±19
33±35
55±41
-1±22
-13±30
-16±32
-15±19
0
6 km
-7 1 10 18 26 34 43 51 60 μGal

changes (after the water table correction) agree within 1 standard deviation at 26 of 32 common gravity sites (Fig. 5), and within 2 standard deviations at 30 out of the 32 sites. Only two sites (CONVICT and 16JCM) appear to have incompatible gravity signals, suggesting the possibility of systematic errors during the occupation of these benchmarks. To emphasize the changes associated with the caldera unrest, and to reduce the possible effect of systematic errors, we average the gravity changes measured between 1982–1998 and 1982–1999 to get a single estimate at each occupied station (Table 3). For simplicity, in the forthcoming text we will refer to this averaged value as the 1982–1999 signal for gravity change, or residual gravity.

During the time period covered by this study (1982–1999), the gravity within the caldera decreased significantly (Fig. 6a), whereas three control stations located on stable granite outcrops more than 5 km outside the caldera show no significant change (Table 3 and Fig. 5). The stations with the largest gravity decrease are all located on the resurgent dome (Fig. 6a), which has experienced significant uplift in the past 20 years (Denlinger and Riley, 1984; Savage et al., 1987; Langbein et al., 1995). In general, these results are in very good qualitative and quantitative agreement with our previously published data (Battaglia et al., 1999). Exceptions are the gravity anomaly centered on the caldera south moat at benchmark A124RST (one station only, not occupied in 1998) and the larger gravity decrease in 1999 at benchmark 4JD (Long Valley plain). It is worth noting that the unusually small gravity change measured at 4JD in 1998 was the cause of a suspicious residual gravity anomaly centered in the Long Valley plain (see Battaglia et al., 1999, fig. 3), an area with minor deformation and no seismic activity. The unusually small raw gravity change (-4 ± 7 μGal) measured in 1998 compared to neighboring stations in the eastern caldera (with gravity changes of -46 ± 10, -30 ± 14, -42 ± 11 μGal) suggests a measurement error at this site during the 1998 survey (see Table 1 and Battaglia et al., 1999). We previously noted that these localized anomalies, associated with single stations, should not be interpreted as significant.

4. Free-air effect and residual gravity

We compute the free-air correction using the vertical displacement field derived by differencing the 1999 GPS survey and the 1982 leveling survey (e.g. Battaglia et al., 2003 – this issue). Only 16 of the 37 occupied gravity stations coincide with a geodetic benchmark. We interpolate the uplift at the remaining stations using kriging (see Appendix 2 for more details). The interpolation error is estimated through sequential Gaussian simulation (Goovaerts, 1997; Deutsch and Journel, 1998). The inflation of the resurgent dome is the most prominent feature of the caldera deformation field (Fig. 6b).

The residual gravity is computed by subtracting the free-air correction from the water-table-corrected gravity change. The residual gravity field (Fig. 6c and Table 3) shows a positive anomaly centered on the resurgent dome with peak amplitude of 59 ± 19 μGal. The anomaly is defined by residual gravity changes of around 50 μGal at three stations (17JCM, 22JCM and 23JCM). Note that these values are significant at the 95% confidence level (2 standard deviations). This positive residual gravity anomaly suggests mass intrusion into the sub-caldera crust beneath the resurgent dome. Other positive anomalies are centered on the caldera south moat (station A124RST, with amplitude 55 ± 41 μGal), and on Mammoth Mountain (stations 5JCM and 3JCM, with amplitudes of 64 ± 34 and 51 ± 31 μGal respectively). These two areas have been the sites of intense unrest (Savage and Cockerham, 1984; Hill et

Fig. 6. (a) Gravity changes from 1982 to 1999, values in μGal, error 1 S.D.; the gravity change reported here is the average of the 1999–82 and 1998–82 measured gravity changes (see Fig. 5), corrected for fluctuations in the water table. (b) Uplift at gravity benchmarks from 1982 to 1999, values in mm, error 1 S.D. (c) Residual gravity from 1982 to 1999, values in μGal, error 1 S.D. The white outline at the center of the caldera is the resurgent dome.

Table 3
Gravity change, uplift, free-air effect and residual gravity in Long Valley caldera from 1982 to 1999

	Gravity change (μGal)	Uplift (mm)	Free-air effect (μGal)	Residual gravity (μGal)
HW 395				
X123	−46 ± 9	206 ± 50	−64 ± 15	18 ± 18
MLEQ03A	−86 ± 13	247 ± 67	−76 ± 21	−10 ± 24
D916	−44 ± 19	295 ± 51	−91 ± 16	47 ± 25
Y123	−56 ± 17	339 ± 36	−105 ± 11	48 ± 20
12DOR75	−119 ± 21	358 ± 51	−111 ± 16	−9 ± 27
MLEQ02	−111 ± 9	379 ± 76	−117 ± 24	6 ± 25
FLOW	−73 ± 9	185 ± 99	−57 ± 31	−16 ± 32
A124RST	−15 ± 20	228 ± 116	−70 ± 36	55 ± 41
CONVICT	−65 ± 6	163 ± 57	−50 ± 17	−15 ± 19
6DOR75	−27 ± 14	115 ± 62	−36 ± 19	8 ± 23
D124	−46 ± 12	99 ± 61	−31 ± 19	−16 ± 22
E124	−21 ± 5	51 ± 62	−16 ± 19	−6 ± 20
MLEQB1	−7 ± 5	84 ± 63	−26 ± 20	19 ± 20
Big loop				
E916	−62 ± 8	223 ± 58	−69 ± 18	7 ± 20
24DOR75	−70 ± 12	155 ± 55	−48 ± 17	−23 ± 20
39DOR75	−46 ± 15	114 ± 56	−35 ± 17	−10 ± 23
2JD1952	−24 ± 11	187 ± 43	−58 ± 13	34 ± 17
MLEQ01	−37 ± 7	179 ± 59	−55 ± 18	19 ± 19
1JD1952	−53 ± 12	167 ± 60	−52 ± 18	−1 ± 22
Small loop				
12JCM82	−85 ± 6	310 ± 55	−96 ± 17	10 ± 18
15JCM82	−80 ± 6	322 ± 54	−100 ± 17	19 ± 18
16JCM82	−87 ± 5	356 ± 27	−110 ± 8	23 ± 10
17JCM82	−71 ± 6	423 ± 60	−131 ± 19	59 ± 19
22JCM82	−79 ± 7	415 ± 28	−128 ± 9	49 ± 11
23JCM82	−92 ± 8	458 ± 6	−141 ± 2	50 ± 8
Antelope Valley Rd				
25JCM82	−106 ± 7	316 ± 72	−97 ± 22	−8 ± 23
Benton Crossing				
3JD1952	−33 ± 12	97 ± 50	−30 ± 15	−3 ± 20
4JD1952	−19 ± 18	69 ± 61	−21 ± 19	2 ± 26
HW 203				
5JCM82	−9 ± 24	238 ± 74	−73 ± 23	64 ± 33
3JCM82	−41 ± 22	299 ± 74	−92 ± 23	51 ± 31
2JCM82	−61 ± 31	305 ± 53	−94 ± 16	33 ± 35
More stations with alternate				
HOT	−67 ± 7	277 ± 84	−86 ± 26	18 ± 27
MLEQ05	−24 ± 6	199 ± 75	−61 ± 23	37 ± 24
MLEQ14	−97 ± 11	272 ± 91	−84 ± 28	−13 ± 30
Control stations				
MLEQ06	−4 ± 6			
MLEQ11	−8 ± 6			
MLEQ13	−1 ± 5			

The gravity change reported here is the average of the 1999–82 and 1998–82 measured gravity changes (Fig. 5), corrected for fluctuations in the water table (Table 2). Error is 1 S.D.

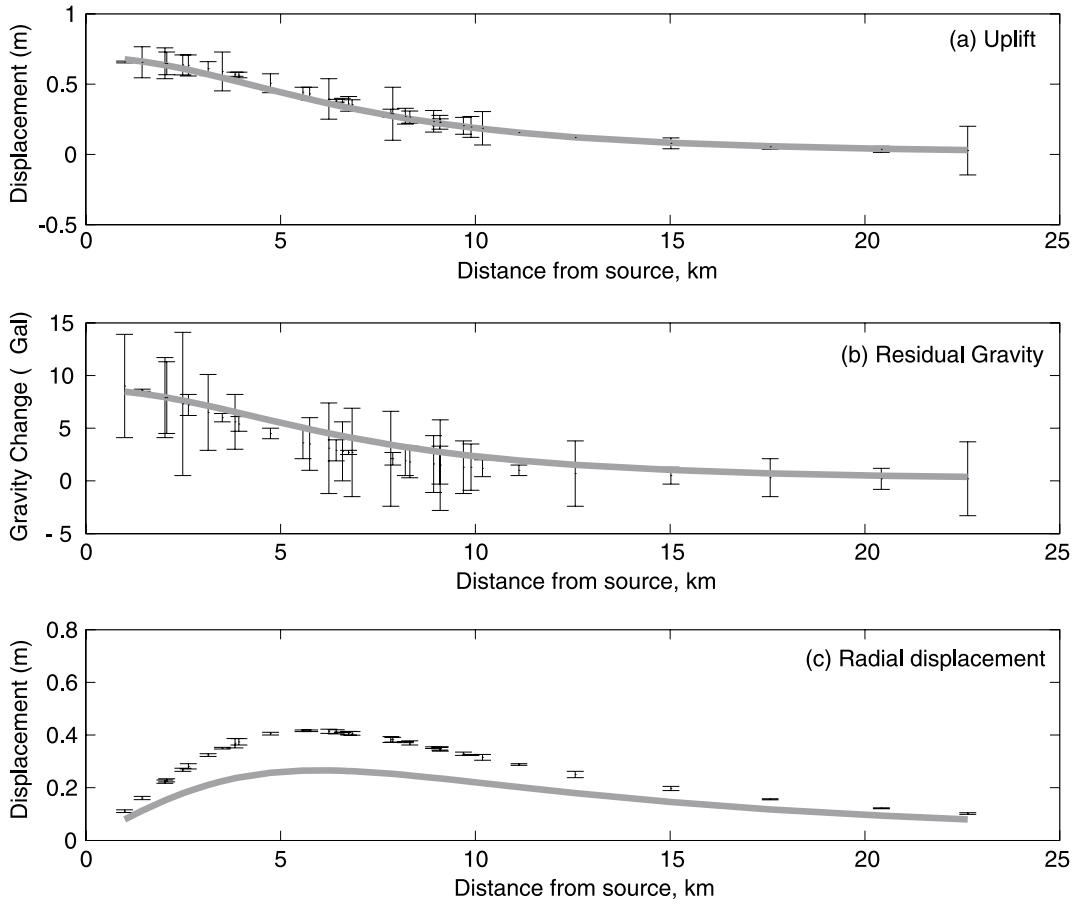

Fig. 7. Bias due to incorrectly assessing the source shape. Fitting a spherical source (solid line) to a data set created using an ellipsoidal source (points+error bars). Uncertainties for the synthetic data set are 6 cm for uplift, 20 μGal for the residual gravity and 6 mm for the radial displacement. This is the same order of magnitude as the errors in the actual data set in Long Valley caldera (Table 3; Appendices 1 and 2 in Battaglia et al., 2003 – this issue). Actual ellipsoidal source: depth = 6 km, volume = 0.2 km^3, mass = 0.5×10^{12} kg, density = 2500 kg/m^3. Inferred spherical source: depth = 8.5 km, volume = 0.2 km^3, mass = 0.9×10^{12} kg, density = 4500 kg/m^3.

al., 1990; Sorey et al., 1993), presumed to be caused by dike intrusions (Savage et al., 1987; Langbein et al., 1995). However, the residual gravity at these three points is not significant at the 95% level, and the anomaly in the south moat is caused by a single station A124RST, so caution is necessary when interpreting these data. Finally, it is worth noting that most of the residual gravity changes outside the resurgent dome are not significant at the 95% confidence level.

When compared to the uplift and residual gravity maps published in Battaglia et al. (1999), the above results confirm the general picture of mass intrusion beneath the resurgent dome proposed there. There are, however, some differences in the details of the vertical deformation and residual gravity fields. The most important are: (a) smaller uplift and residual gravity east of the resurgent dome (Long Valley plain); (b) the shift toward the southern part of the resurgent dome of the positive residual gravity anomaly; (c) the disappearance of the large positive anomaly centered on station 4JD, east of the resurgent dome. These differences can be explained mostly as a consequence of the direct measurement of the caldera uplift in July 1999. We have to keep in mind

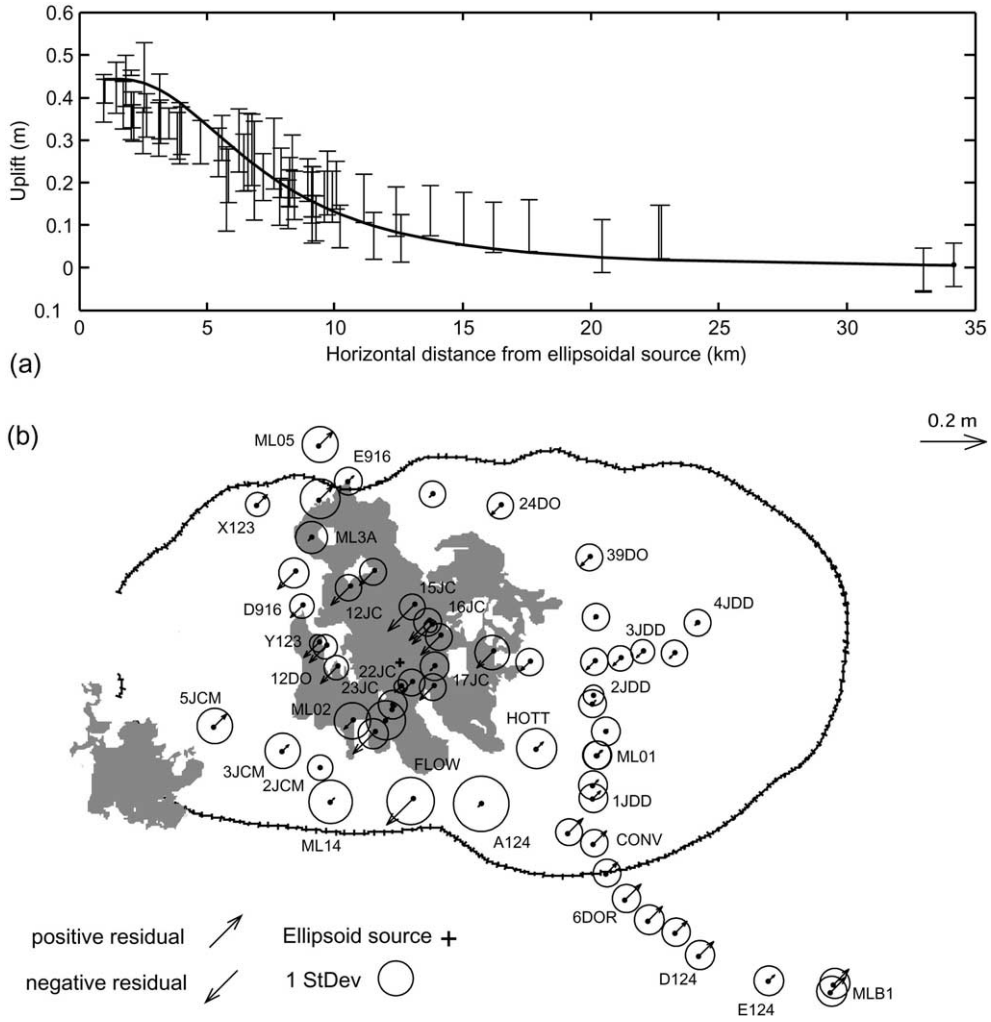

Fig. 8. Fit of ellipsoidal source (depth = 5.9 km, volume change = 0.136 km^3, $b/a = 0.475$) to uplift in Long Valley caldera from 1982 to 1999. (a) Comparison between observed (error bars) and predicted (solid line) uplift at gravity and geodetic benchmarks. (b) Residual distribution (observed−predicted uplift) at gravity benchmarks.

that the most recent leveling survey of the Long Valley plain (benchmarks 3JD and 4JD) dates back to 1988, while the last complete leveling survey of resurgent dome was in 1992. The estimates of caldera uplift by Battaglia et al. (1999), based on geostatistical or elastic models, probably overestimated the vertical displacement in these areas. The disappearance of residual gravity anomaly centered on the Long Valley plain represents an important improvement of our field measurements with respect to our previously published data (Battaglia et al., 1999). This anomaly was based on a single data point (4JD), and was therefore not significant.

5. Modeling the intrusion

Estimates of the density of the intrusion in volcanic areas are usually computed by matching gravity and uplift data to a point source model (Hagiwara, 1978; Eggers, 1987; Fernandez and Rundle, 1994; Rymer, 1994). One of the major shortcomings of this approach is that we may fit

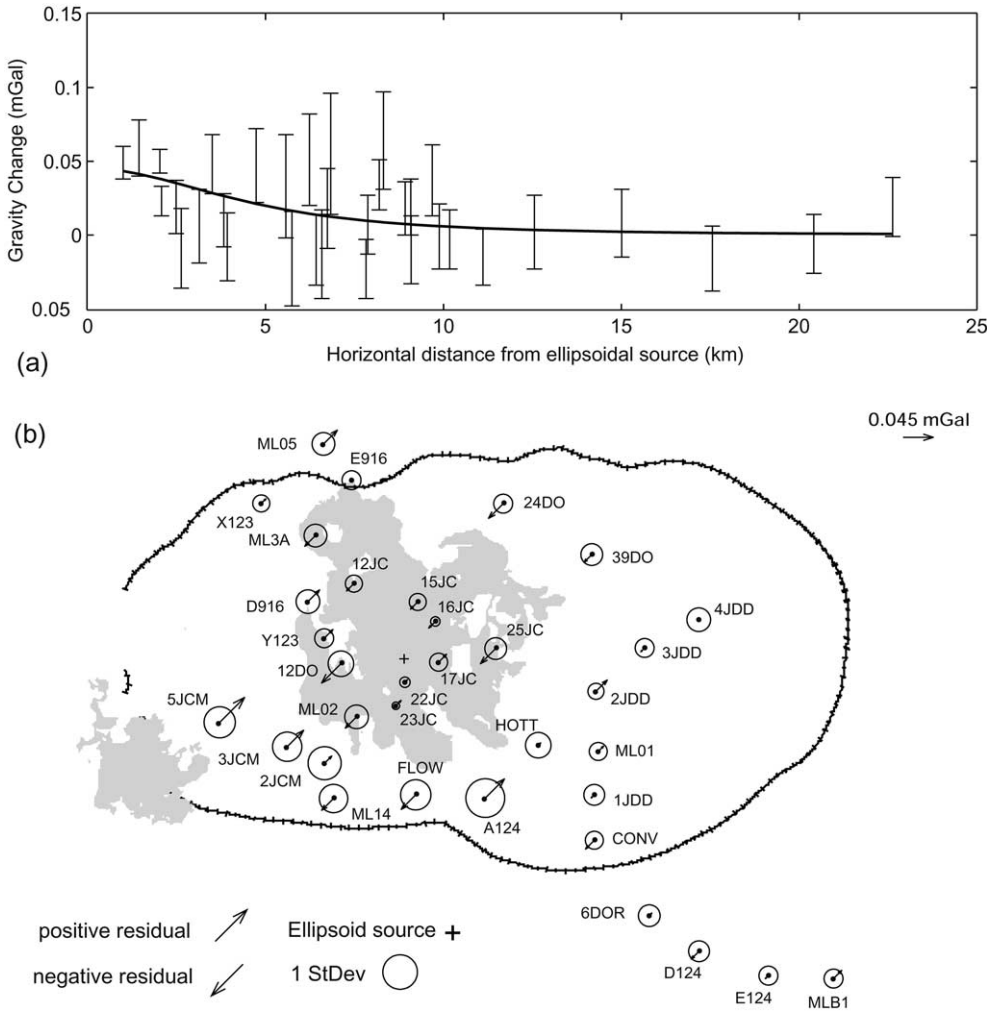

Fig. 9. Fit of ellipsoidal source (depth = 5.9 km, volume = 0.136 km^3, $b/a = 0.475$, mass = 0.233 MU and density = 1713 kg/m^3) to residual gravity. (a) Comparison between observed (error bars) and predicted (solid line) residual gravity. (b) Residual distribution (observed−predicted residual gravity).

the wrong model to the experimental data set, because different elastic models produce very similar vertical deformations (e.g. Dieterich and Decker, 1975). This will yield estimates of the density and depth of the intrusion that are not reliable. Let us consider, for example, synthetic data from an ellipsoidal source incorrectly modeled by a spherical source. Modeling the uplift with a spherical source fits the data well but predicts a deeper location for the intrusion (e.g. Table 7 in Battaglia et al., 2003 – this issue), requiring a larger mass to obtain the same gravity signal. However, the estimated volume increase is close to the correct value, because the spherical source is more efficient in causing vertical deformation. The net effect is that we overestimate the density of the intrusion by incorrectly assuming a spherical source. This is shown by the example in Fig. 7, where we fit a spherical model to uplift and residual gravity data predicted by an ellipsoidal model (Fig. 7a,b). The spherical model fit appears reasonable and is able to explain about 99% of the uplift and gravity data. Unfortunately, it overestimates the source depth by 2.5 km (30%)

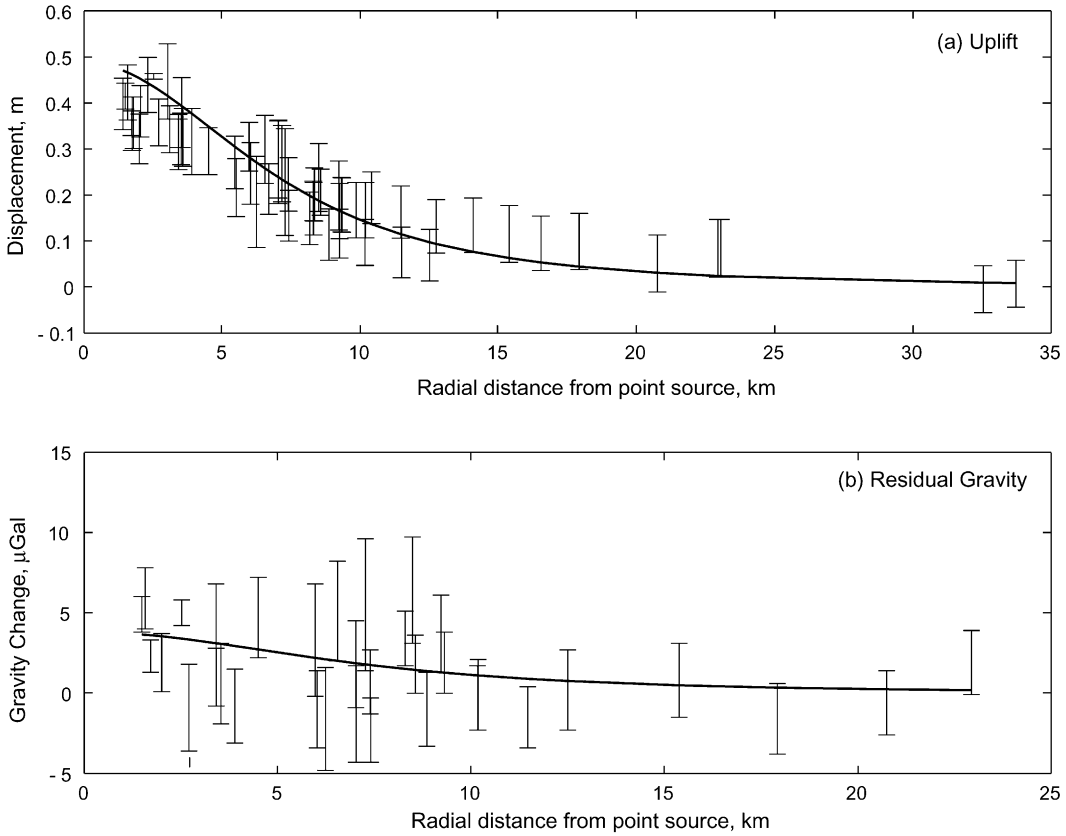

Fig. 10. Fit of a spherical source (solid line) to Long Valley caldera (a) uplift and (b) residual gravity (error bars). This fit gives a caldera inflation source with a depth $d = 8.8$ km (33% increase), a volume change from 1982 to 1999 $\Delta V = 0.155$ km^3 (14% increase) and a density $\rho \approx 2883$ kg/m^3 (40% increase). The spherical source has the same horizontal position as the ellipsoidal source.

and its density by 2000 kg/m^3 (44%). It is only when we compare the radial displacements (Fig. 7c) that we realize that the spherical model is not appropriate. We conclude that in order to obtain a reliable estimate of the depth and density of the intrusion, inversion of geodetic and gravity data must include not only the uplift and residual gravity, but the horizontal deformation as well.

Given the constraints of the available geodetic and gravity data sets (uplift data are available from 1975, gravity data from 1982, but horizontal deformation data only from 1985), and the need to have the largest possible signal-to-noise ratio, our modeling strategy follows a two-step approach.

First we invert vertical and horizontal displace-

Table 4
Density of supercritical fluids (after Zhang and Frantz, 1987)

Depth (km)	T (°C)	P (kbar)	Density (kg/m^3)			
			H_2O	H_2O KCl	H_2O NaCl	H_2O $CaCl_2$
4.9	375	1.3	750	850	850	950
7.5	575	2.0	600	750	750	800

All binary fluids are 2.0 molal solutions.

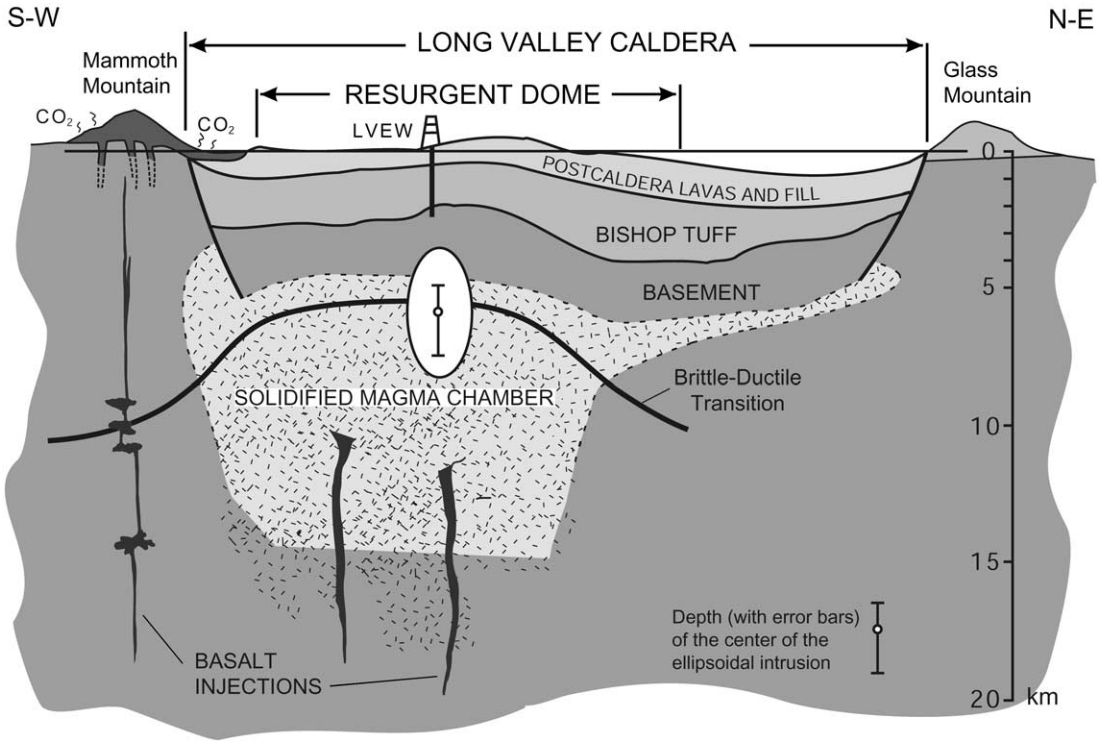

Fig. 11. Cross-section of Long Valley caldera (modified from Sackett et al., 1999) showing the location of the intrusion. LVEW marks the location of the Long Valley exploratory well. The present-day shallow hydrothermal system consists of several relatively thin zones of hot water, flowing laterally from west to east at depth of less than 1 km (Sorey, 1985; Sorey et al., 1991). The dimensions of the ellipsoidal intrusion are speculative and based on an overpressure $\Delta P \approx 1$ Gpa and shear modulus $\mu \approx 30$ GPa.

ments from 1985 to 1999 for a vertical prolate ellipsoidal source in elastic, homogeneous, isotropic half-space (Yang et al., 1988) to constrain position, depth and geometry of the source (see Battaglia et al., 2003 – this issue). The main source of deformation is found to be a prolate ellipsoid located beneath the resurgent dome at a depth $d = 5.9$ km (95% bounds of 4.9–7.5 km), with an aspect ratio $A = 0.475$ (95% bounds are 0.25–0.65) (Battaglia et al., 2003 – this issue).

Using the above ellipsoidal source, we invert uplift (Fig. 8) and residual gravity data (Fig. 9) from 1982 to 1999 using a weighted least-squares algorithm to constrain the volume, mass and thus density of the source. The expression for the residual gravity signal due to a prolate ellipsoid of revolution in elastic, homogeneous, isotropic half-space is presented in Appendix 3. The fit of the model to the experimental data is quite good (Figs. 8 and 9). We obtain an intrusion mass of 0.233 MU (1 MU = 10^{12} kg), a volume change $\Delta V = 0.136$ km^3 and a density $\rho \cong 1700$ kg/m^3 for the intrusion. We use a bootstrap percentile method (Efron and Tibshirani, 1986) to obtain 95% confidence bounds on the parameters of the ellipsoidal model. The method yields 95% bounds of 0.139–0.376 MU on mass, 0.105–0.187 km^3 on volume change, and 1180–2330 kg/m^3 on density.

It is worth noting that a spherical source would have fit the uplift and residual gravity data reasonably well (Fig. 10; e.g. Battaglia et al., 1999), giving a caldera inflation source with a depth $d = 8.8$ km (a 33% increase), a volume change $\Delta V = 0.155$ km^3 (a 14% increase) and a density $\rho = 2883$ kg/m^3 (a 40% increase). These values

fall within the 95% bounds determined by Battaglia et al. (1999) using a point source to invert gravity and geodetic data from 1982 to 1998: depth 6.9–18.3 km; volume change 0.11–0.54 km^3; density 2.7–4.0$\times 10^3$ kg/m^3.

6. Constraining the source of unrest

To discriminate between magmatic or aqueous fluid intrusion as the source of unrest in the Long Valley area, we compare the estimated density with densities of magmas and aqueous fluids at appropriate pressure and temperature conditions. First we need to determine the pressure and temperature with depth beneath the resurgent dome so that we can set a density range for the aqueous fluids. A caldera cross-section (Fig. 11) shows that the intrusion is located within the solidified remnants of the magma chamber. Assuming an average density for the crust of 2700 kg/m^3, the pressure range corresponding to the depth of the inflation source is 1.3–2.0 kbar (0.13–0.2 GPa). A temperature range of 375–575°C can be inferred using data from geothermal wells (Sorey, 1985). Note that this estimate is quite conservative, because this temperature range corresponds to a conductive heat flow of 160 mW m^{-2}, about one-fourth of the average caldera heat flow (Sorey, 1985). Higher temperatures correspond to even lower densities of the aqueous fluids. At these pressures and temperatures, aqueous fluids are supercritical. Limited data for the density of a supercritical fluid with the composition of geothermal brine are available in the literature (Potter and Haas, 1978; Zhang and Frantz, 1987). The available experimental data (Table 4) show a density range for such fluids from a minimum of 600 kg/m^3 to a maximum of 950 kg/m^3 (Zhang and Frantz, 1987). This density range falls below the 95% lower bound (1180 kg/m^3) estimated for the density of the intrusion beneath the resurgent dome, but only by 20%.

The distribution of S- and P-wave attenuation (Q_S^{-1}, Q_P^{-1}) and the ratio of P- and S-wave velocities (V_P/V_S) indicates the existence of deep hydrothermal zones at the margins of the resurgent dome, but no major deep hydrothermal system beneath the resurgent dome (Sanders et al., 1995). This is another indication that the perturbation of a deep hydrothermal system beneath the resurgent dome is not likely to be the primary cause of unrest at Long Valley caldera.

Given that our results do not support the intrusion of hydrothermal fluids as the primary cause of unrest at Long Valley caldera, what can we infer about the nature of the source beneath the resurgent dome? The density of silicate melts can be determined by the evaluation of the quotient (Spera, 2000):

$$\rho = \sum X_i M_i / V(T, P, X) \tag{2}$$

where X_i is the mole fraction, M_i is the molar mass, and V the partial molar volume of the melt. To a good approximation, V can be taken independent of composition and only as a function of temperature T and pressure P. So, we can use a relatively simple empirical equation of state to compute V and the melt density (Spera, 2000):

$$V(T, P, X) = \sum X_i [V_{i,T_r} + (\partial V_i/\partial T)(T - T_r) + (\partial V_i/\partial P)(P - P_r)] \tag{3}$$

where T_r and P_r are constant reference conditions (generally 1673 K and 10^{-4} Gpa, 1 bar, respectively), and V_i is the partial molar volume of the ith component. Volcanic rocks are quenched relatively rapidly and thus provide more or less direct information regarding the composition of natural melts (Spera, 2000). So, we may roughly estimate possible compositions of silicic melts of the present Long Valley magmatic system from rhyolites erupted after the caldera-forming eruption (see Table 5). Another important factor in determining the melt density is the amount of dissolved H_2O. Small amounts of dissolved water may dramatically lower melt densities (Scarfe, 1986). If two parcels of saturated granitic melt were trapped at pressures of 2 and 1 kbar, respectively, the water content at 900°C would be ~6 and 4 wt% (Burnham, 1997). Melt densities (calculated at a pressure of 1.6 kbar –5.9 km depth – and 900°C – liquidus temperature for granitic

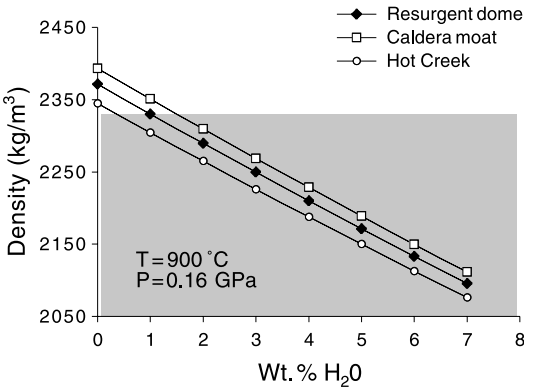

Fig. 12. Melt density as a function of dissolved water content for post-caldera rhyolites from Long Valley (see Table 5). 900°C is the liquidus temperature of a granitic melt. 0.16 GPa is the lithostatic pressure corresponding to a depth of 5.9 km. The gray area identifies all the density values below the upper 95% bound (2330 kg/m^3) for the density of the intrusion.

melts) are portrayed graphically as a function of temperature in Fig. 12. Melts with a content of dissolved water above 1 wt% H_2O fall within the 95% upper bound (2330 kg/m^3) of the estimated intrusion density. Available data on the pre-eruption water contents of Long Valley rhyolitic magmas give about 4 wt% H_2O for samples from Obsidian Dome (Mono-Inyo craters; Hervig et al., 1989), about 5 wt% H_2O in melt inclusions from the Bishop Tuff (Wallace et al., 1999), and 3 wt% H_2O for samples from the caldera (Taylor et al., 1983).

7. Summary and discussion

Our results indicate that it is possible to use geodesy and gravity to discriminate between magmatic and aqueous fluid intrusions in silicic calderas. In the case of Long Valley caldera, the data do not support the intrusion of hydrothermal fluids as the primary cause of unrest. Gravity data do, however, support the intrusion of silicic magma, or a hybrid magma–fluid body, beneath the resurgent dome. Comparison between estimated bounds on the intrusion density and melt densities suggests the possibility of rhyolitic magma intrusion. There is additional evidence for intrusion beneath Mammoth Mountain and the caldera south moat. Unfortunately, the residual gravity signal in these two sites is not significant at the 95% level, so caution is necessary when interpreting these data.

Choosing the right model to invert geodetic and gravity data is a critical step in the geological interpretation of the data set. Since sources with different geometries have similar vertical deformation patterns (e.g. Dieterich and Decker, 1975), both horizontal and vertical displacements must be used to determine the geometry of the intrusion. If the source does not possess a spherical symmetry, the standard approach of using a point source to invert uplift and gravity data will lead to biased estimates of the source parameters. In the case of Long Valley caldera, a spherical source provides a reasonably good fit to the uplift and

Table 5
Mole fractions X_i, molar masses M_i, partial molar volumes V_i, thermal expansions dV_i/dT and compressibilities dV_i/dP of oxide components of post-caldera rhyolites from Long Valley

Oxide	X_i (a)	X_i (b)	X_i (c)	M_i (10^{-3} kg/mol)	V_i (10^{-6} m^3/mol)	dV_i/dT (10^{-9} m^3/mol K)	dV_i/dP (10^{-6} m^3/mol GPa)
SiO_2	0.815	0.793	0.852	60.08	26.86	0	−1.89
TiO_2	0.002	0.003	0.001	79.88	23.16	7.24	−2.31
Al_2O_3	0.088	0.092	0.073	102.96	37.42	0	−2.26
Fe_2O_3	0.006	0.009	0.003	159.69	42.13	9.09	−2.53
MgO	0.003	0.009	0.001	40.3	11.69	3.27	0.27
CaO	0.011	0.018	0.006	56.08	16.53	3.74	0.34
Na_2O	0.039	0.045	0.032	61.98	28.88	7.68	−2.4
K_2O	0.036	0.031	0.033	94.02	45.07	12.08	−6.57
H_2O	–	–	–	18.02	26.27	9.46	−3.15

After Heumann and Davies (1997); Spera (2000).
Rhyolite sample location: (a) resurgent dome (Qef); (b) caldera moat (Qmr); (c) hot creek (Qmrh). After Bailey (1989).

residual gravity data (Fig. 10), but overestimates the source depth by 2.9 km (33% increase), the volume change by 0.019 km^3 (14% increase) and the density by about 1200 kg/m^3 (40% increase). The biased density estimate would point to a mafic intrusion rather than a silicic intrusion (e.g. Battaglia et al., 1999).

Even if the ellipsoidal model defined in this paper provides a more realistic representation of the Long Valley caldera inflation source than a point source model (in the sense that such a model fits the geodetic and gravity data better than a point source), there are other factors that should be taken into account when discussing the interpretation of our results, and that can probably be the basis for future work.

The first is that the crust is not a homogeneous half-space. A layered Earth model, with one or more elastic layers, may be more realistic, although lateral variations also exist. Deformation changes the gravitational field in two ways: dilatational strains change the local density, and displacements perturb any density contrasts, especially at the free surface (e.g. Bonafede and Mazzanti, 1998). How important are these effects?

In Battaglia and Segall (2004), we investigated two factors that should help in obtaining a more realistic picture of the intrusive body: (1) coupling between elastic and gravitational effects (e.g. Fernandez et al., 2000); (2) a layered Earth model, with depth-dependent elastic properties and densities (e.g. Fernandez and Rundle, 1994). Our results show that coupling between elastic and gravitational effects (self-gravitation) is second-order over the distance and time scales normally associated with volcano deformation. We find no significant differences in any of the source parameters due to self-gravitation effects. For an elastic model appropriate to Long Valley caldera, we find only minor differences when modeling the intrusion using a point source in a homogeneous or layered medium. Choosing the right source model to invert geodetic and gravity data, however, is critical in the geological interpretation of the data. If the source does not possess spherical symmetry, the standard approach of using a point source to invert uplift and gravity data will lead to biased estimates of the source parameters (e.g. a deeper location and a larger density). Our results support the intrusion of silicate melts, but leave considerable uncertainty about the nature of the magma chamber and intruding fluid. For example, is the ellipsoidal model a representation of a real geological structure (e.g. a neck or volcanic plug intruding into the shallow crust) or are we just visualizing some sort of average properties (depth, volume, mass, density) of the real geological structure? If we are measuring average properties, then the low density estimated for the intrusion (1180–2330 kg/m^3) could point to a hybrid source composed of melt and a separate aqueous phase. Many hydrothermal ore deposits are generated by hydrothermal fluids that contain a component of magmatic fluids along with heated groundwater (Hedenquist and Lowenstern, 1994). In addition, the volume of alteration and

Table 6
Fit of single and hybrid sources to geodetic and residual gravity (Res G) data

Source		A	d	Geodetic data (1985–99)					Geodetic and gravity data (1982–99)						
				ΔV	χ^2		R^2		ΔV	ΔM MU	ρ	χ^2		R^2	
			(km)	(km^3)	Uplift	EDM	Uplift	EDM	(km^3)		(kg/m^3)	Uplift	Res G	Uplift	Res G
Spherical		1	8	0.12	228	239	0.08	0.98	0.13	0.38	2900	61	36	0.99	0.67
Ellipsoidal		0.48	5.9	0.09	67	267	0.73	0.98	0.14	0.23	1700	65	34	0.99	0.68
Hybrid	Fluid	1	6.4	0.03	124	753	0.50	0.94	0.04	0.03	700	114	48	0.98	0.55
	Melt	1	7.4	0.05					0.07	0.17	2400				

All sources have the same position: (332 188, 4 172 064) in UTM (NAD27) coordinates. The average density for the hybrid source is around 1800 kg/m^3.

A, aspect ratio; d, depth; ΔV, volume change; ΔM, mass change; ρ, density; EDM, horizontal displacement from two-color EDM data; Res G, residual gravity; R^2, goodness of fit: if $R^2 = 1$, the model is able to explain all variation in the observed data, if $R^2 = 0$, the model is not able to explain the observed data.

amount of ore metal suggest that intrusions into the shallow crust may be accompanied by degassing of a larger volume of subjacent magma (Guilbert and Park, 1986, p. 109).

A possible first step towards a hybrid representation of the inflation source is to move from a single source to a binary source. For example, we can fit geodetic and gravity data from Long Valley using a very simple hybrid source composed of two spherical sources, a deeper magma body and a shallower aqueous phase (e.g. Norton and Cathles, 1973). We assume for simplicity that the parameters (mass, volume, depth) of these two sources should fall within the 95% bounds of the ellipsoid source. A possible solution consists of an upper source 6.4 km deep with a density of 700 kg/m^3 simulating the fluid intrusion, and a lower source 7.4 km deep with a density of 2400 kg/m^3 representing the silicic melt intrusion. Note that we are not looking here for the optimal fit, but exploring possible interpretations of the inferred density (1700 kg/m^3). Table 6 gives a summary of how well this hybrid model compares with single source models. The hybrid model fits the 1985–1999 geodetic data reasonably well (see Table 6). The fit is not as good as the ellipsoidal model, but gives a far better match to the vertical deformation than the spherical model. Regarding the 1982–1999 geodetic and gravity data (see Table 6), the goodness of fit (R^2) for the uplift is practically the same for all models, while the fit to the gravity data is slightly inferior for the hybrid model. The average density for the hybrid model is around 1800 kg/m^3. Fluids represent about 15% of the total mass of the intrusion. Even if this very simple hybrid model is not as efficient as the ellipsoidal model in fitting the data set, nevertheless it offers a geologically plausible description of the intrusion (e.g. Norton and Cathles, 1973). Spatially distributed models, as well as those with depth-varying density, should be the subject of future research.

Acknowledgements

This work would not have been possible without the support and data from several individuals and institutions. In particular we would like to thank: R. Bailey, D. Dzurisin and T. Elliot (Cascades Volcano Observatory), C. Farrar (U.S. Geological Survey), D. Hill and J. Langbein (Long Valley Observatory), J. Murray and A. Fernandez for field assistance, Y. Fialko for providing the ellipsoidal source code, M. Zumberge, G. Sasagawa and R. Jachens for discussion. Support provided by the USGS Volcano Hazard Program and the DoE, Office of Basic Energy Science, DE-FG03-99ER14962.

Appendix 1. Water table correction to gravity

If we approximate an aquifer with an infinite slab, the associate gravity change will be:

$$\Delta g = 2\pi G \Delta m \tag{4}$$

where G is the gravitational constant and Δm the change in mass per unit surface area. In the case of an unconfined aquifer, we have:

$$\Delta m = \phi_e \rho_w \delta z \tag{5}$$

where ϕ_e is the effective porosity of the unconfined aquifer, ρ_w the water density and δz the change in the water table. For a confined aquifer the change in mass is (Fetter, 1988, p. 107):

$$\Delta m = S \rho_w \phi_z \tag{6}$$

where S is the storativity of the confined aquifer and ϕ_z the change in the piezometric head. If we substitute the values for G and ρ_w in Eqs. 4–6, we obtain:

$$\Delta g_{WT} = 42 \phi_e \delta z \ \mu\text{Gal} \quad \Delta g_\phi = 42 S \phi_z \ \mu\text{Gal} \tag{7}$$

Typical values for the porosity in Long Valley shallow aquifers range from 0.05 for granite to 0.45 for the caldera fill (Sorey et al., 1978). Values of storativity S for tuffaceous rocks similar to the caldera-confined hydrothermal aquifers range from 4×10^{-3} (Geldon, 1993) to 5×10^{-4} (Geldon, 1999). This implies that Δg_{WT} is 10–1000 times larger than Δg_ϕ.

Appendix 2. Geostatistical models

In this Appendix, we briefly describe the practical steps necessary to develop and apply space–time interpolation. For more details about the theory of geostatistics, readers are referred to Isaak and Srivastava (1989), Rouhani and Myers (1990), Deutsch and Journel (1998) and Kyriakidis and Journel (1999). We use kriging to interpolate uplift (or water table changes) at unsampled gravity benchmarks. To apply kriging, we follow a step by step approach.

First, we compute the experimental variogram (Isaak and Srivastava, 1989, p. 60; Deutsch and Journel, 1998, p. 43) from the field data (Fig. 13a, uplift; Fig. 13c, water table). The variogram is the key to any geostatistical study. It measures the average variability between data values separated by a distance h. We have one experimental variogram for the uplift (we measure only the spatial variability; Fig. 13a), and two experimental variograms for the water table change (we measure both spatial and temporal variability; Fig. 13c).

We fit a theoretical model (Isaak and Srivastava, 1989, Ch. 16; Deutsch and Journel, 1998, p. 25) to the experimental variogram (Fig. 13a, uplift; Fig. 13c, water table). Variogram models can be divided into two types: those that reach a plateau (sill) and those that do not. The distance at which they reach this plateau is called the range. For example, the Gaussian model, fitting the experimental variogram in Fig. 13a, reaches a sill of 0.28 at a range of 6 km. The variogram discontinuity at the origin is called the nugget effect. More than one theoretical model can fit the experimental variogram (e.g. in Fig. 13a, the Gaussian model offers a good fit of the experimental data between 2.5 and 5 km, but the power model better fits the far field trend; in Fig. 13c, the time component shows a periodicity that we fit by a hole effect model, while we propose two alternative models for the space component):

Gaussian model (range a, sill c):

$$\gamma(h) = c[1-\exp(-(3h^2/a^2))] \quad (8)$$

Power model ($0<w<2$, positive slope c):

$$\gamma(h) = ch^w \quad (9)$$

Hole effect model (range a, sill c):

$$\gamma(h) = c[1-\cos(\pi h/a)] \quad (10)$$

We choose the best model using cross-validation (Isaak and Srivastava, 1989, ch. 15). In cross-validation, actual data are dropped one at a time and re-estimated using the remaining neighboring data. Each datum is replaced in the data set once it has been re-estimated. We accept the model with statistical distribution closest to the original data, and with the higher correlation between true and estimated values. For example, the choice of the uplift interpolation model is straightforward because the power model (see Fig. 13a) has a higher correlation between the true and interpolated values than the Gaussian model, 0.94 against 0.76 (Fig. 13b). On the other hand, we have no such clear distinction for the water table, Fig. 13d, so the choice of the interpolation model is somewhat arbitrary. It is worth noting that cross-validation can detect possible problems; it does not ensure that the interpolation will give 'realistic' results (Journel, 1989).

Finally, unsampled values (uplift or water table change) are estimated using ordinary kriging (Deutsch and Journel, 1998, p. 63). The kriging algorithm provides a minimum error-variance estimate of the unsampled value. Kriging tends to smooth out details and extreme values of the original data set when used as a mapping algorithm (see Fig. 6).

A sequential Gaussian simulation algorithm (Deutsch and Journel, 1998, p. 144) is applied to estimate the uncertainty of kriging interpolations. A simulation realizes a large number of estimates of the variable of interest at an unsampled location. The standard deviation of the estimated distribution is taken as a measure of the error of the interpolation. The simulation of a variable using the Gaussian algorithm proceeds as follows.

First, we decluster the data set, if necessary. Data are often spatially clustered (i.e. data have been heavily sampled in some selected locations). To obtain a representative statistical distribution

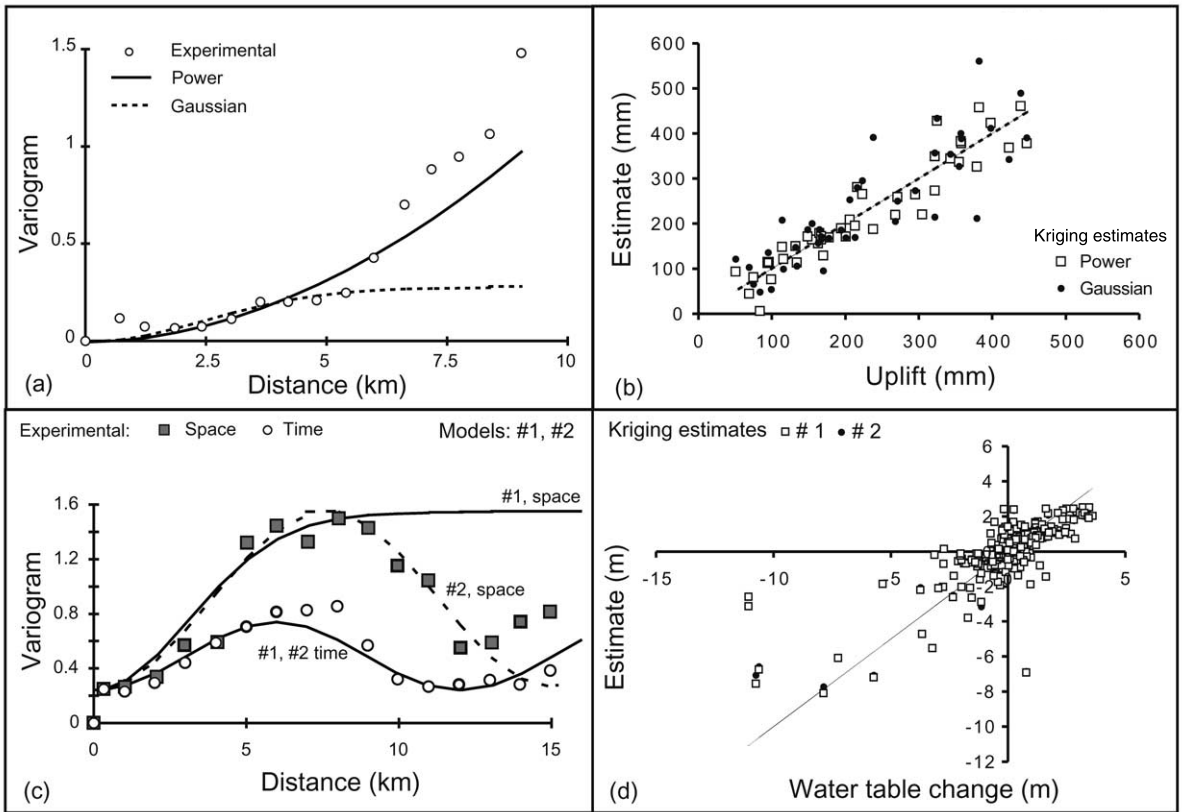

		Variogram modeling			Model cross-validation		
	Model	Nugget	Sill	Range	Mean	St Dev	Correlation
Uplift					**232**	**113**	
	Gaussian	0.00	0.280	6.0	231	133	0.76
	Power	*0.00*	*0.015*	*1.9*	*229*	*118*	*0.94*
Water table change					**-0.002**	**1.622**	
	#1, space (gaussian)	*0.25*	*1.300*	*7.5*	*0.007*	*1.28*	*0.779*
	#1, time (hole)	*0.25*	*0.250*	*6.0*			
	#2, space (hole)	0.25	0.650	7.5	0.006	1.252	0.776
	#2, time (hole)	0.25	0.250	6.0			

Fig. 13. Geostatistical models for space–time interpolation. Uplift: (a) variograms; (b) cross-validation. Water table change: (c) variograms; (d) cross-validation. The power model was used to interpolate the uplift, and the model #1 to interpolate the water table change.

of the entire area of interest, declustering weights are assigned, such that values in areas with more data receive less weight than those in sparsely sampled areas (Deutsch and Journel, 1998, p. 213). For example, the mean and cumulative probability of the original uplift data set (Fig. 14a) is smaller than those of the declustered data set (Fig. 14b), indicating that geodetic data have been preferentially sampled in areas of higher deformation (i.e. original mean = 222 mm, declustered mean = 151 mm).

The Gaussian simulation works with data that follow a normal distribution. Unfortunately, most Earth science data do not follow a normal distri-

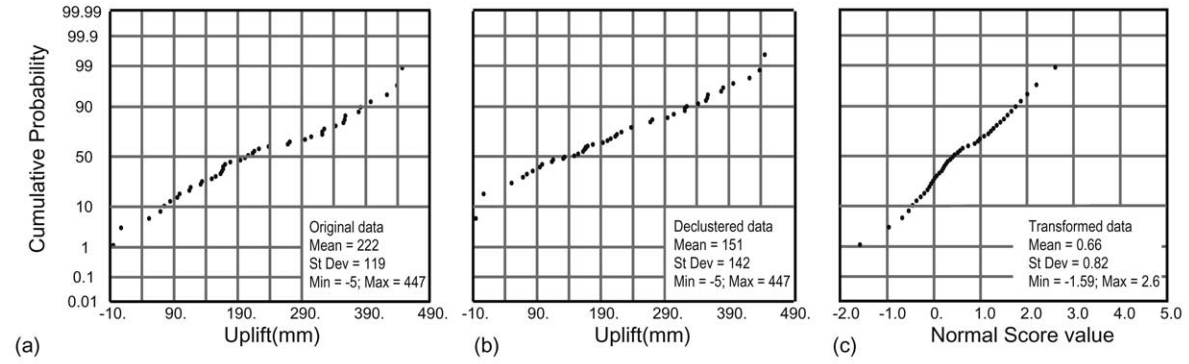

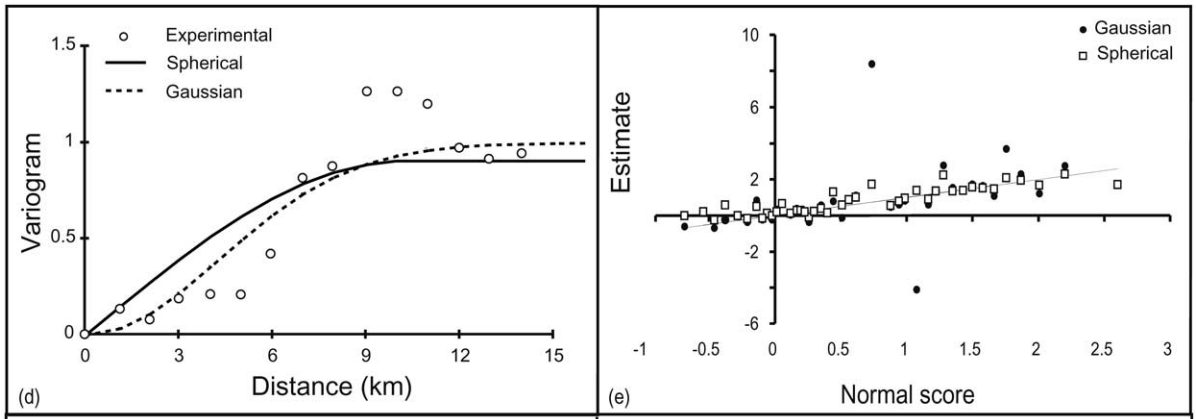

Variogram modeling				Model cross-validation			
Model	Nugget	Sill	Range	Data set	Mean	St Dev	Correlation
				Normal score	0.66	0.82	
Gaussian	0.00	1.0	10.5	Kriged (Gaussian)	0.80	1.70	0.47
Spherical	*0.00*	*0.9*	*10.0*	*Kriged (spherical)*	*0.80*	*0.74*	*0.87*

Fig. 14. Geostatistical models for sequential Gaussian simulation of uplift: (a) original data set; (b) declustered data set; (c) transformed data set (normal score) used in the simulation; (d) transformed data set (normal score) variogram models; (e) cross-validation. The spherical model was chosen to estimate the interpolation error of uplift. The interpolation error of the water table change was estimated using a Gaussian model (sill = 0.4, range = 9) in space, and a hole model (sill = 0.2, range = 6) in time.

bution. This is not a major problem since a non-linear transformation can transform the original (or declustered) data distribution (Fig. 14b) into a normal distribution (Fig. 14c). The transformed data set is also called normal score. The simulation is performed in the normal space, then the simulated values are back-transformed (Deutsch and Journel, 1998, p. 141)

Just as in kriging, the variogram model is the key to any Gaussian simulation. Two models (Gaussian and spherical) fit the experimental normal score variogram (Fig. 14d). Cross-validation (Fig. 14e) indicates that the best interpolation results are obtained using the spherical model:

Spherical model (range a, sill c) :

$$y(h) = c\begin{cases} 1.5h/a - 0.5(h/a)^3 & h<a \\ 1 & h\geq a \end{cases} \qquad (11)$$

Finally, multiple realizations (around 100) of the transformed variable are performed using the sequential Gaussian simulation algorithm (Deutsch and Journel, 1998, p. 139). Every realization is then back-transformed using the declus-

tered data distribution. At any sampled point, the simulation algorithm returns the exact experimental value. Post-processing allows estimating the point-to-point standard deviation of the realizations.

Appendix 3. Residual gravity of a prolate ellipsoid of revolution

The residual gravity component at the (x,y) location for a vertically elongated prolate ellipsoid of revolution is (Clark et al., 1986):

$$\Delta g_R = 3G\frac{\Delta M}{(1-A^2)^{1.5}}\frac{d}{a}\left\{\log\left[\frac{(1-A^2)^{0.5}+(1-\lambda)^{0.5}}{(A^2+\lambda)^{0.5}}\right]-\left[\frac{1-A^2}{1+\lambda}\right]^{0.5}\right\} \quad (12)$$

where λ is the largest of the three real roots of:

$$s^3+p_2s^2+p_1s+p_0=0$$

$$p_2=1+2A^2-\underline{d}^2-L^2$$

$$p_1=2A^2+A^4-2A^2\underline{d}^2-(1+A^2)L^2$$

$$p_0=A^4-A^4\underline{d}^2-A^2L^2$$

$$\underline{d}=d/a,\ L^2=(x^2+y)/a^2 \quad (13)$$

and a is the ellipsoid semi-major axis, b the semi-minor axis, $A=b/a$, $\underline{d}$ the (positive) depth of the ellipsoid center, x and y the horizontal coordinates with respect to the ellipsoid major axis.

References

Amelung, F., Jonsson, S., Zebker, H., Segall, P., 2000. Widespread uplift and 'trapdoor' faulting on Galapagos volcanoes observed with radar interferometry. Nature 407, 993–996.

Arnet, F., Kahle, H., Klingele, E., Smith, R., Meertens, C., Dzurisin, D., 1997. Temporal height and gravity changes of the Yellowstone caldera, 1977-1994. Geophys. Res. Lett. 24, 2741–2744.

Bailey, R.A., 1989. Geologic map of Long Valley Caldera, Mono-Inyo Craters volcanic chain, and vicinity, eastern California, Map I-1933, US Geol. Survey, Reston.

Bailey, R.A., Hill, D.P., 1990. Magmatic unrest at Long Valley Caldera, California, 1980-1990. Geosci. Can. 17, 175.

Barberi, F., Cassano, E., La Torre, P., Sbrana, A., 1996. The problem of volcanic unrest; the Campi Flegrei case history. In: Scandone, R. (Ed.), Monitoring and Mitigation of Volcano Hazards. Springer, Berlin, pp. 771–786.

Battaglia, M., Segall, P., 2004. The interpretation of gravity changes and crustal deformation in active volcanic areas. Pure Appl. Geophys., 161 (7).

Battaglia, M., Roberts, C., Segall, P., 1999. Magma intrusion beneath Long Valley Caldera confirmed by temporal changes in gravity. Science 285, 2119–2122.

Battaglia, M., Segall, P., Murray, M., Cervelli, P., Langbein, J., 2003. The mechanics of unrest at Long Valley caldera, California: 1. Modeling the geometry of the source using GPS, leveling and two-color EDM data. J. Volcanol. Geotherm. Res. 127, 195–217.

Berrino, G., Rymer, H., Brown, G.C., Corrado, G., 1992. Gravity-height correlations for unrest at calderas. J. Volcanol. Geotherm. Res. 53, 11–26.

Berrino, G., 1994. Gravity changes induced by height-mass variations at the Campi Flegrei caldera. J. Volcanol. Geotherm. Res. 61, 293–309.

Bonafede, M., 1991. Hot fluid migration; an efficient source of ground deformation; application to the 1982-1985 crisis at Campi Flegrei-Italy. J. Volcanol. Geotherm. Res. 48, 187–198.

Bonafede, M., Mazzanti, M., 1998. Modelling gravity variations consistent with ground deformation in the Campi Flegrei caldera (Italy). J. Volcanol. Geotherm. Res. 81, 137–157.

Burnham, C.W., 1997. Magma and hydrothermal fluids. In: Barnes, H.L. (Ed.), Geochemistry of Hydrothermal Ore Deposits. Wiley, New York, pp. 63–124.

Clark, D.A., Saul, S.J., Emerson, D.W., 1986. Magnetic and gravity anomalies of a triaxial ellipsoid. Explor. Geophys. 17, 189–200.

Del Gaudio, C., Ricciardi, G.P., Ricco, C., Sepe, V., Borgstrom, S., Cecere, G., De Martino, P., D'Errico, V., Siniscalchi, V., Aquino, I., Tesauro, M., 2001. Livellazione di precisione. In: Rendiconto sull'attivita' di sorveglianza INGV Osservatorio Vesuviano, II semestre (Luglio - Dicembre 2000), Napoli, Italy, Internal Report, pp. 41–47.

De Natale, G., Pingue, F., Allard, P., Zollo, A., 1991. Geophysical and geochemical modelling of the 1982-1984 unrest phenomena at Campi Flegrei Caldera (southern Italy). J. Volcanol. Geotherm. Res. 48, 199–222.

Denlinger, R.P., Riley, F.S., 1984. Deformation of Long Valley Caldera, Mono County, California, from 1975 to 1982. J. Geophys. Res. 89, 8303–8314.

Deutsch, C.V., Journel, A.G., 1998. GSLIB. Geostatistical Software Library and User's Guide. Oxford University Press, New York.

Dieterich, J.H., Decker, R., 1975. Finite element modeling of

surface deformation associated with volcanism. J. Geophys. Res. 80, 4094–4102.
Dixon, T., Mao, A., Bursik, M., Heflin, M., Langbein, J., Stein, R., Webb, F., 1997. Continuous monitoring of surface deformation at Long Valley Caldera, California, with GPS. J. Geophys. Res. 102, 12017–12034.
Dvorak, J.J., Dzurisin, D., 1997. Volcano geodesy: the search for magma reservoirs and the formation of eruptive vents. Rev. Geophys. 35, 343–384.
Dzurisin, D., Yamashita, K.M., Kleinman, J., 1994. Mechanisms of crustal uplift and subsidence at the Yellowstone Caldera, Wyoming. Bull. Volcanol. 56, 261–270.
Dzurisin, D., Savage, J., Fournier, B., 1990. Recent crustal subsidence at Yellowstone Caldera, Wyoming. Bull. Volcanol. 52, 247–270.
Efron, B., Tibshirani, R., 1986. Bootstrap methods for standard errors, confidence intervals, and other measures of statistical accuracy. Statist. Sci. 1, 54–77.
Eggers, A., 1987. Residual gravity changes and eruption magnitudes. J. Volcanol. Geotherm. Res. 33, 201–216.
Ewert, J.W., Lockhart, A.B., Marcial, S., Ambubuyog, G., 1996. Ground deformation prior to the 1991 eruptions of Mount Pinatubo. In: Newhall (Ed.), Fire and Mud; Eruptions and Lahars of Mount Pinatubo, Philippines. Philippine Institute of Volcanology and Seismology, pp. 329–338.
Fetter, C.W., 1988. Applied Hydrogeology. Merrill Publ. Co., Columbus.
Fernandez, J., Rundle, J., 1994. Gravity changes and deformation due to a magmatic intrusion in a two-layered crust model. J. Geophys. Res. 99, 2737–2746.
Fernandez, J., Charco, M., Tiampo, K.F., Jenttzsch, G., Rundle, J.B., 2000. Joint interpretation of displacement and gravity data in volcanic areas. A test example: Long Valley caldera, California. Geophys. Res. Lett. 28, 1063–1066.
Geldon, A.L., 1993. Analysis of aquifer tests in Miocene tuffaceous rocks having layered fracture and matrix permeability, Yucca Mountain, Nevada. Geol. Soc. Am. 25, 257.
Geldon, A.L., 1999. An 18-month pumping test in Miocene tuffaceous rocks at Yucca Mountain, Nevada; methods and results. Geol. Soc. Am. 31, 148.
Goovaerts, P., 1997. Geostatistics for Natural Resources Evaluation. Oxford University Press, New York.
Guilbert, J.M., Park Jr., C.F., 1986. The Geology of Ore Deposits. Freeman, New York.
Hagiwara, Y., 1978. Gravity changes associated with seismic activity. Earthquake precursors; Proceedings of the US-Japan Seminar on Theoretical and Experimental Investigations of Earthquake Precursors, Tokyo, pp. 137–146.
Hedenquist, J.W., Lowenstern, J.B., 1994. The role of magmas in the formation of hydrothermal ore deposits. Nature 370, 519–527.
Hervig, R.L., Dunbar, N., Westrich, H.R., Kyle, P., 1989. Pre-eruptive water content of rhyolitic magmas as determined by ion microprobe analyses of melt inclusions in phenocrysts. J. Volcanol. Geotherm. Res. 36, 293–302.
Heumann, A., Davies, G.R., 1997. Isotopic and chemical evolution of the post-caldera rhyolitic system at Long Valley, California. J. Petrol. 38, 1661–1678.
Hill, D.P., 1998. 1998 SSA meeting; Presidental address; Science, geologic hazards, and public in a large, restless caldera. Seism. Res. Lett. 69, 400–404.
Hill, D.P., Ellsworth, W.L., Johnston, M.S., Langbein, J.O., Oppenheimer, D.H., Pitt, A.M., Reasenberg, P.A., Sorey, M.L., McNutt, S.R., 1990. The 1989 earthquake swarm beneath Mammoth Mountain, California; an initial look at the 4 May through 30 September activity. Bull. Seismol. Soc. Am. 80, 325–339.
Howle, J., Farrar, C., 1996. Hydrologic data for Long Valley Caldera, Mono County, California, 1978-93. Open-File Report, U.S. Geological Survey, OF 96-0382.
Isaak, E.H., Srivastava, R.M., 1989. Applied Geostatistics. Oxford University Press, New York.
Jachens, R., 1979. Temporal gravity changes as applied to studies of crustal deformation. Open-File Report, U.S. Geological Survey, OF 79-0370, pp. 222–243.
Jachens, R., Roberts, C., 1985. Temporal and areal gravity investigations at Long Valley Caldera, California. J. Geophys. Res. 90, 11210–11218.
Jachens, R., Spydell, R., Pitts, S., Dzurisin, D., Roberts, C., 1982. Temporal gravity variations at Mount St. Helens, March-May 1980. In: Mullineaux, D. (Ed.), 1980 Eruptions of Mount St. Helens, Washington. U.S. Geological Survey Professional Paper 1250, pp. 175–181.
Journel, A., 1989. Fundamentals of geostatistics in five lessons. In: Crawford, M. (Ed.), Short Course in Geology 8. American Geophysical Union, Washington, DC.
Kuo, J.T., Ottaviani, M., Singh, S.K., 1969. Variations of vertical gravity gradient in New York City and Alpine, New Jersey. Geophysics 34, 235–248.
Kyriakidis, P., Journel, A., 1999. Geostatistical space-time models: a review. Math. Geol. 31, 651–683.
Langbein, J., Dzurisin, D., Marshall, G., Stein, R., Rundle, J., 1995. Shallow and peripheral volcanic sources of inflation revealed by modeling two-color geodimeter and leveling data from Long Valley Caldera, California, 1988-1992. J. Geophys. Res. 100, 12487.
Martini, M., Giannini, L., Buccianti, A., Prati, F., Legittimo, P., Iozzelli, P., Capaccioni, B., 1991. 1980-1990; ten years of geochemical investigation at Phlegrean Fields (Italy). J. Volcanol. Geotherm. Res. 48, 161–171.
McKee, C., Mori, J., Talai, B., 1989. Microgravity changes and ground deformation at Rabaul caldera, 1973-1985. In: Latter, J. (Ed.), IAVCEI Proceedings in Volcanology. Springer, Berlin, pp. 399–431.
Nishi, K., Ono, H., Mori, H., 1999. Global positioning system measurements of ground deformation caused by magma intrusion and lava discharge: the 1990-1995 euption at Unzendake volcano, Kyushu, Japan. J. Volcanol. Geotherm. Res. 89, 23–34.
Norton, D.L., Cathles, L.M., 1973. Breccia pipoes, products of exsolved vapor from magmas. Econ. Geol. 68, 540–546.
Orsi, G., Petrazzuoli, S.M., Wohletz, K., 1999. Mechanical and thermo-fluid behaviour during unrest at the Campi Fle-

grei Caldera (Italy). J. Volcanol. Geotherm. Res. 91, 453–470.

Owen, S., Segall, P., Lisowski, M., Miklius, A., Murray, M., Bevis, M., Foster, J., 2000. January 30, 1997 eruptive event on Kilauea Volcano, Hawaii, as monitored by continuous GPS. Geophys. Res. Lett. 27, 2757.

Potter, R.W., Haas, J.L., 1978. Models for calculating density and vapor pressure of geothermal brines. J. Res. U.S. Geol. Surv. 6, 247–257.

Roberts, C., Jachens, R., Morin, R., 1988. High-precision stations for monitoring gravity changes in Long Valley Caldera, California. Open-File Report, U.S. Geological Survey, OF 88-0050.

Rouhani, S., Myers, D., 1990. Problems in space-time kriging of geohydrological data. Math. Geol. 22, 611–623.

Rundle, J., Whitcomb, J., 1986. Modeling gravity and trilateration data in Long Valley, California, 1983-1984. J. Geophys. Res. 91, 12675–12682.

Rymer, H., 1994. Microgravity change as a precursor to volcanic activity. J. Volcanol. Geotherm. Res. 61, 311–328.

Rymer, H., Williams-Jones, G., 2000. Volcanic eruption precursors: Magma chamber physics from gravity and deformation measurements. Geophys. Res. Lett. 27, 2389–2392.

Sackett, P.C., McConnell, V.S., Roach, A.L., Priest, S.S., Sass, J.H., 1999. Long Valley coring Project, 1998. Preliminary stratigraphy and images of recovered core. U.S. Geol. Survey Open-File Report, pp. 99–158.

Sanders, C.O., Ponko, S.C., Nixon, L.D., Schwartz, E.A., 1995. Seismological evidence for magmatic and hydrothermal structure in Long Valley caldera from local earthquake attenuation and velocity tomography. J. Geophys. Res. 100, 8311–8326.

Savage, J., Cockerham, R.S., 1984. Earthquake swarm in Long Valley Caldera, California, January 1983; evidence for dike inflation. J. Geophys. Res. 89, 8315–8324.

Savage, J., Cockerham, R.S., Estrem, J.E., Moore, L.R., 1987. Deformation near the Long Valley Caldera, eastern California, 1982-1986. J. Geophys. Res. 92, 2721–2746.

Scarfe, C.M., 1986. Viscosity and density of silicate melts. In: Scarfe, M.H. (Ed.), Silicate Melts; Their Properties and Structure Applied to Problems in Geochemistry, Petrology, Economic Geology and Planetary Geology. Mineralogical Association of Canada, Toronto, pp. 36–49.

Sorey, M., 1985. Evaluation and present state of the hydrothermal system in Long Valley caldera. J. Geophys. Res. 90, 11219–11228.

Sorey, M., Lewis, R.E., Olmsted, F.H., 1978. The hydrothermal system of Long Valley caldera, California. U.S. Geological Survey Professional Paper, P 1044-A.

Sorey, M.L., Kennedy, B.M., Evans, C.W., Farrar, C.D., Suemnicht, G.A., 1993. Helium isotope and gas discharge variations associated with crustal unrest in Long Valley Caldera, California, 1989-1992. J. Geophys. Res. 98, 15871–15889.

Spera, F.J., 2000. Physical properties of magma. In: Sigurdsson, H. (Ed.), Encyclopedia of Volcanoes. Academic Press, San Diego, CA, pp. 171–190.

Taylor, B.E., Eichelberger, J.C., Westrich, H.R., 1983. Hydrogen isotopic evidence of rhyolitic magma degassing during shallow intrusion and eruption. Nature 306, 541–545.

Tilling, R., Dvorak, J., 1993. Anatomy of a basaltic volcano. Nature 363, 125–133.

Voight, B., Hoblitt, R.P., Clarke, A.B., Lockhart, A.B., Miller, AngusD., Lynch, L., McMahon, J., 1998. Remarkable cyclic ground deformation monitored in real-time on Montserrat, and its use in eruption forecasting. Geophys. Res. Lett. 18, 3405–3408.

Yang, X., Davis, P.M., Dieterich, J.H., 1988. Deformation from inflation of a dipping finite prolate spheroid in an elastic half-space as a model for volcanic stressing. J. Geophys. Res. 93, 4249–4257.

Wallace, P., Anderson, A., Davis, A.M., 1999. Gradients in H_2O, CO_2, and exsolved gas in a large volume silicic magma system: Interpreting the record preserved in melt inclusions from the Bishop Tuff. J. Geophys. Res. 104, 20097–20122.

Walsh, J., Rice, J., 1979. Local changes in gravity resulting from deformation. J. Geophys. Res. 84, 165–170.

Wang, Y., 1997. Theoretical modeling of local gravity changes and deformation caused by dilatancy with the magmatic intrusion. IAG Symposia 117, 289–296.

Wicks, C., Thatcher, W., Dzurisin, D., 1998. Migration of fluids beneath Yellowstone Caldera inferred from satellite radar interferometry. Science 282, 458–462.

Zhang, Y., Frantz, J.D., 1987. Determination of the homogenization temperatures and densities of supercritical fluids in the system NaCl-KCl-$CaCl_2$-H_2O using synthetic fluid inclusions. Chem. Geol. 64, 335–350.